PHILIPS LABORATORIES, INC.

Irvington-on-Hudson, New York

Research Laboratory

TECHNICAL REPORT NO. 34

August 15, 1950

Case No. 4500

I. THERMIONIC EMISSION FROM OXIDE CATHODES;
II. PHOTOCONDUCTIVITY IN SEMICONDUCTORS

by

E. S. RITTNER

Approved

O. S. Duffendack

O. S. Duffendack
Director of Research

Approved for Distribution

F. M. Vogel

F. M. Vogel
Manager, Patent Department
August 15, 1950

PREFACE

This report represents a supplement to Technical Report No. 25 entitled, "Concerning Some Aspects of Solid State Theory." Section I of the present report supersedes section VIII B of the previous report, which passed into obsolescence about the time of printing; whereas section II contains new information not covered previously.

The material of this report also represents substantially the content of five lectures delivered by the author during the week of August 7, 1950 at the Summer Electronics Symposium on Semiconductor Electronics sponsored by the University of Michigan.

TABLE OF CONTENTS

Page

INTRODUCTION

It is the purpose of the present series of lectures to discuss two specific topics, namely thermionic emission from oxide cathodes and photoconductivity in semiconductors. Both subjects have something in common in the sense that although the original discoveries were made many decades ago, even at the present time a complete understanding of these phenomena are not yet at hand. For this reason our procedure will be to present a somewhat chronological account of the more important pictures that have been advanced up to the present time.

I. THERMIONIC EMISSION FROM OXIDE CATHODES

1. Facts

Oxide cathodes usually are comprised of alkaline earth oxides, notably BaO, and preferably BaO-SrO mixtures. The oxides are coated (by spraying or by cataphoresis, etc.) on metal bases (usually Ni) in the form of carbonates, which are subsequently decomposed to the oxides by heating in vacuo at high temperatures. In order to produce good electron emitters, a further process called "activation" is required. Before activation the resistance and work function are both quite high (megohms and a few e.v. respectively). Activation usually consists of further heat treatment in vacuo. It is accelerated by incorporating small amounts of electropositive metals in the base metal or by drawing emission current. In the latter case oxygen is evolved at a rate which

diminishes as activation proceeds. The activated cathode is semiconducting and exhibits a low work function ($\sim$ 1 e.v.). It is, however, highly susceptible to poisoning by O_2 or H_2O vapor (but not by inert gases).

2. Early Explanation

We shall skip hastily over the early pictures which were advanced to explain the behavior of oxide cathodes and summarize the situation as it existed in the mid-thirties (see de Boer[1]). At that time it was thought that Ba atoms were adsorbed on active spots of surface of the cathode. The high electrostatic fields at these points were supposed to lower the ionization potential by a Stark effect so that the Baatoms could be thermally ionized at much lower temperatures than are required for free Ba atoms. Since this picture was not susceptible to a quantitative development, we shall not deal with it further here.

3. Simple Semiconductor Model

With the development of wave mechanics and its application to solids followed by the further application of Fermi statistics, the situation became ripe for explaining the oxide cathode behavior in terms of a semiconductor picture and all the more recent explanations have been of this variety.* The qualitative idea is that activation removes

*For a review of the situation as of 1939 and 1948 see references 2) and 3), respectively.

a small quantity of oxygen, leaving behind a stoichiometric excess of barium in the lattice. This is accelerated by contact with electropositive metals owing to their affinity for oxygen. (In fact interface oxide compounds have been found in many cases, but this is probably only a complicating but relatively unimportant feature.) Electron emission activates by electrolytic action, oxygen gas being evolved at the surface and free Ba being plated out at the metal base. A stoichiometric excess of Ba in the lattice represents a source of extra electrons which can be freed more readily than normally bound electrons. The analogue in an energy scheme is shown in the accompanying sketch. The quantity χ (called the electron affinity of the crystal) represents the energy separation between the bottom of the conduction band and a point outside the solid. χ arises from the attraction by the positive ions of the crystal for the free electrons and also from the presence of surface double layers. Since in the activation process an insulator is converted to a semiconductor, this explains why the resistance and work function decrease so markedly.

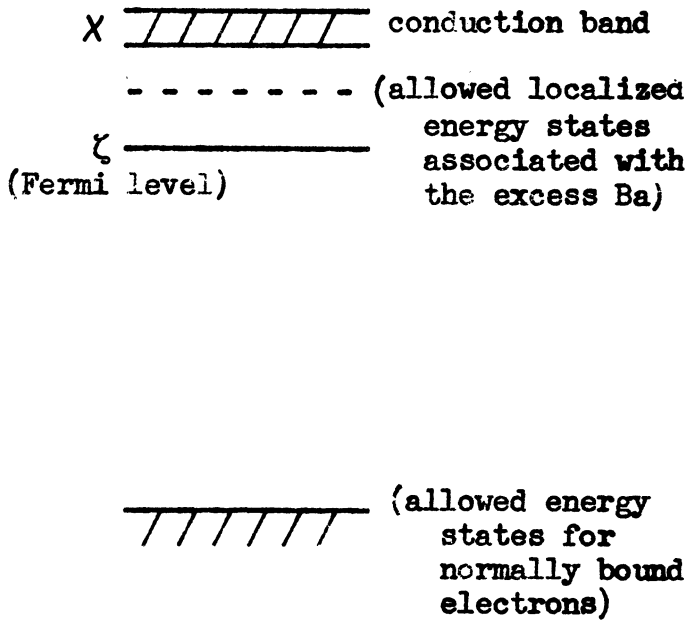

4. Quantitative Theory for Simple Model

The question then arises as to what success this picture has when put on a quantitative basis? There are two quantities we wish to calculate: I, the thermionic emission current density, and σ, the electrical conductivity. We also wish to know the dependence on temperature and activation of these quantities.

A previous lecturer has already derived the general thermionic emission formula (see also Philips Technical Report No. 25, p. 277)

$$I = A(1-r)T^2 e^{-\phi/kT} = \frac{2(2\pi m_e e k^2)}{h^3}(1-r)T^2 e^{-\phi/kT} ,$$

which is applicable here if ϕ is taken to represent the energy separation between the Fermi level, ζ, and a point outside the cathode (i.e. $\phi = \chi - \zeta$).

With respect to σ, by definition $\sigma = n_e e b$, the mobility b (drift velocity per unit fieldstrength in the field direction) is difficult to calculate, but since it is n_e (the number of free electrons per unit volume in the material) which changes markedly with temperature and activation we shall focus attention on it. A previous lecturer has shown already that

$$n_e = \frac{2(2\pi m_e kT)^{3/2}}{h^3} e^{\zeta/kT}$$

and we shall also reprove this in a moment.

Thus, if we assume a semiconductor model (including a value of χ), we can determine the Fermi level position and in turn I and n_e (which is proportional to σ). Consider the model

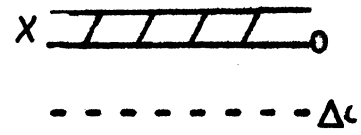

At T = 0°K, let N_d = number of electrons/cm^3 in impurity levels. Then, since the space charge = 0,

$$n(E)f(E)dE = N_d \tag{1}$$

where n(e)dE is the number of energy states/cm^3 with energies between E and E + dE and f(e) = probability of occupation =

$$\frac{1}{e^{E-\zeta/kT} + 1} \tag{2}$$

for Fermi Dirac statistics (which apply to electrons). Divide the integral into two regions. For $E > 0$, assuming a free electron gas

$$n(E) = \frac{4\pi}{h^3}(2m_e)^{3/2} E^{1/2} \tag{3}$$

(see Seitz[4], pp. 140-143).

For $E < 0$ let n(E) at the impurity level be represented by a Dirac δ-function

$$n(E) = N_d\delta(E + \Delta\varepsilon_d) \tag{4}$$

Substituting (3) and (4) into (1),

$$\frac{4\pi}{h^3}(2m_e)^{3/2}\int_o^\infty \frac{E^{1/2}dE}{e^{(E-\zeta)/kT}+1} + \int_{-\infty}^{o} \frac{N_d\delta(E+\Delta\varepsilon_d)dE}{e^{(E-\zeta)/kT}+1} = N_d \qquad (5)$$

The first term of eq. (5) cannot be directly integrated. However, if the Fermi level is several kT or more below the bottom of the conduction band, it is possible to neglect the 1 in the denominator, which is equivalent to the use of Boltzmann statistics. Taking out of the integral the constant quantity $e^{\zeta/kT}$, defining a new variable $x = E/kT$ (which yields $(kT)^{3/2}$ outside the integral), we obtain an integral of the form $\int_o^\infty \frac{\sqrt{x}\,dx}{e^x}$ which has the known value $\sqrt{\pi}/2$. Thus, the integration of eq. (5) yields

$$\frac{4\pi(2m_e)^{3/2}e^{\zeta/kT}(kT)^{3/2}\sqrt{\pi}}{h^3\quad 2} + \frac{N_d}{e^{-(\Delta\varepsilon_d-\zeta)/kT}+1} = N_d \qquad (6)$$

or substituting

$$P = \frac{2(2\pi m_e kT)^{3/2}}{h^3}$$

$$Pe^{\zeta/kT} = N_d\left(1 - \frac{1}{e^{(-\Delta\varepsilon_d/kT-\zeta)/kT}+1}\right) \qquad (7)$$

$$Pe^{\zeta/kT} = N_d\left(1 - \frac{e^{\zeta/kT}}{e^{-\Delta\varepsilon_d/kT}+e^{\zeta/kT}}\right)$$

$$= \frac{N_d e^{-\Delta\varepsilon_d/kT}}{e^{-\Delta\varepsilon_d/kT}+e^{\zeta/kT}} = n_e \qquad (8)$$

---

*Note that from the following equations

(a) $n_e = Pe^{\zeta/kT}$

(b) $n_o = n_e e^{-\chi/kT}$ (Boltzmann eq.), where n_o = density of free electrons outside solid

(c) $(1-r)n_o e = I(2\pi m/kT)^{1/2}$ (from kinetic theory)

one can readily derive the general emission equation.

If the same procedure had been carried out with additional unfilled levels of density Na at a separation $-\Delta\varepsilon_a$ and a full band at $-\Delta E$, the following expression (needed later) would have been obtained: (see reference 5) for complete details).

$$\underbrace{Pe^{\zeta/kT}}_{n_e} = \underbrace{\frac{N_d e^{-\Delta\varepsilon_d/kT}}{e^{-\Delta\varepsilon_d/kT} + e^{\zeta/kT}}}_{\text{density of bound holes in donors}} - \underbrace{\frac{N_a e^{\zeta/kT}}{e^{-\Delta\varepsilon_a/kT} + e^{\zeta/kT}}}_{\text{density of bound electrons in acceptors}} + \underbrace{Qe^{(-\zeta/kT - \Delta E/kT)}}_{n_h} \qquad (9)$$

where $Q = \dfrac{2(2\pi m_h kT)^{3/2}}{h^3}$

Eq. (8) is a quadratic equation for $e^{\zeta/kT}$, which is the quantity needed in the emission equation and in the equation for n_e (and hence σ). The solution is

$$e^{\zeta/kT} = \frac{e^{-\Delta\varepsilon_d/kT}}{2}\left[-1 + \left(1 + \frac{4N_d}{P} e^{\Delta\varepsilon_d/kT}\right)^{1/2}\right] \qquad (9a)$$

There are now two interesting cases:

(a) $\dfrac{4N_d}{P} e^{\Delta\varepsilon_d/kT} >> 1$

(b) $\dfrac{4N_d}{P} e^{\Delta\varepsilon_d/kT} << 1$

In case (a) we have

$$e^{\zeta/kT} = \sqrt{\frac{N_d}{P}}\, e^{-\Delta\varepsilon_d/2kT} \qquad (10)$$

Substituting into the emission eq.,

$$I = \frac{2(2\pi m_e e k^2)}{h^3}(1-r)T^2 e^{-\chi/kT} \frac{(N_d)^{1/2} h^{3/2}}{\sqrt{2}(2\pi m_e kT)^{3/4}} e^{-\Delta\varepsilon_d/2kT}$$

$$= \frac{\sqrt{2}(2\pi m_e)^{1/4} e(kT)^{5/4}(1-r) N_d^{1/2} e^{(-\Delta\varepsilon_d/2 + \chi)/kT}}{h^{3/2}} \tag{11}$$

and also

$$n_e = P_e^{\zeta/kT} = \sqrt{N_d P}\, e^{-\Delta\varepsilon_d/2kT} = N_d^{1/2}\sqrt{2}\left(\frac{2\pi m_e kT}{h^{3/2}}\right)^{3/4} e^{-\Delta\varepsilon_d/2kT} \tag{12}$$

In case (b) developing $(1+x)^{1/2} = 1 + 1/2\, x$ we have

$$e^{\zeta/kT} = \frac{N_d}{P}$$

Therefore

$$I = \frac{2(2\pi m_e e k^2)}{h^3}(1-r)T^2 e^{-\chi/kT} \frac{N_d h^3}{2(2\pi m_e kT)^{3/2}}$$

$$= (2\pi m_e)^{-1/2} e(1-r)(kT)^{1/2} N_d e^{-\chi/kT} \tag{13}$$

and

$$n_e \cong N_d \tag{14}$$

(complete ionization)

The behavior of the Fermi level for this model may be seen in Fig. 1 which shows ζ vs. T for $\Delta\varepsilon_d$ = 0.2 e.v. below the conduction band, and for $N_d = 10^{17}$, 3×10^{17}, and $10^{18}/cm^3$. In the lower temperature

region, case (a) is valid (Fermi level several kT's below conduction band and several kT's above donor level). At high temperatures where the Fermi level is well below the donor level, case (b) is valid. When the Fermi level is just at the donor position, the donors are fifty per cent ionized, as is immediately obvious from the definition of the Fermi level.

Fig. 2 shows a plot of log n_e against $10^4/T$ corresponding to the three Fermi level curves of Fig. 1. At low temperatures, in the validity range of case (a), eq. (12) is valid and the slope of the straight lines constitute a measure of $\Delta\varepsilon_d$. At high temperatures where case (b) applies, complete ionization of the donors occurs, in accordance with eq. (14).

5. Test of Simple Theory

In order to decide which of these equations to use and in order to apply them, it is necessary to know N_d, $\Delta\varepsilon_d$, and χ. These can only be obtained from experiment. N_d is determined by direct chemical analysis. Ba and H_2O vapor $\longrightarrow H_2$, which is measured volumetrically. In a well-activated cathode N_d is found to be $3 \times 10^{17}/cm^3$, which represents an excess of barium of about ten parts per million. If eq. (12) applies, since b does not vary rapidly with T compared to n_e, then from a plot of log σ vs. 1/T, one measures $\Delta\varepsilon_d$. In early experiments log σ vs. 1/T plots gave single straight lines with a slope yielding a value for $\Delta\varepsilon_d$ of about 1.4 e.v. For these values of $\Delta\varepsilon_d$ and N_d and over the normal operating temperature range of the cathode,

$$\frac{4N_d}{P} e^{\Delta\varepsilon_d/kT} \geq 10^6$$

and Kawamura[6] and very detailed experiments by Hannay, MacNair and White[8], yield the results shown in Fig. 3 which implies that χ is independent of activation.

Thus, the simple semiconductor picture seems to have had marked success; it could account for the then observed temperature dependence of σ and I and gave a not too unreasonable calculated value for I. It also implied χ independent of activation, which is appealing because of its simplicity. It failed, however, to account for the gradual change in Richardson work function and apparent $\Delta\varepsilon_d$ with activation which has been generally observed (Mott's explanation of interaction between impurities seems unreasonable on the basis of the large interaction energy required (ca 1 e.v.) in view of the small magnitude of N_d), and it could not explain more recent data (that of Vink and Loosjes[9]), and of Wright[11] and Morgulis and Iagovdik[12] to be discussed below.

6. Pore Conduction Hypothesis

The situation has been materially altered by the recent work of Vink and Loosjes[9] who extensively investigated the conductivity over a wider temperature range than that employed previously. Their technique was to measure the conductivity of the configuration shown in the sketch by means of an A.C. Wheatstone Bridge, with a low applied voltage. Their results, which are shown in Fig. 4 as a plot of log resistance vs. 1/T, indicate three separate regions: I (between about 600 and 800°K) of low slope, II (between about 800 and 1000°K) of steeper slope, and III a part of gradually diminishing slope (above about 1000°K). The slope in regions

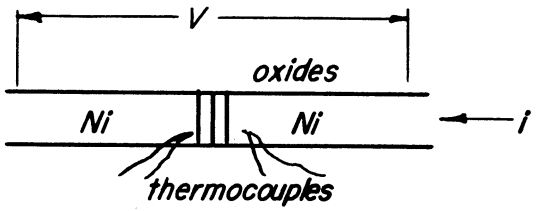

I and II decrease progressively with activation. (In region I the slope can be as low as 0.1 e.v.). Previous workers covered small temperature ranges and this data is generally in agreement with most previous published data. They further measured i-V characteristics up to ca 500 V/cm. In region I the i-V characteristics were found to be linear, in region II they were curved toward the voltage axis, and in region III they were linear again. It is clear that the simple semiconductor model outlined above will not explain this data.

The explanation given by Vink and Loosjes of their data stems from a consideration of the effect of pores. The cathodes studied by them are typical of commercial cathode ray gun cathodes made by spraying and are very porous (50-60% porosity). It is only to be expected that at higher temperatures the pores will be filled with an electron gas due to thermionic emission and that this gas can contribute to the conductivity. Thus, one expects two parallel conduction mechanisms, through the semiconducting grains and through the pores via the electron gas. The latter may become important at high temperature because the effective conduction area as well as the mean free path increase greatly for this process. The slope of log R vs. 1/T curves are in accord with the notion of two parallel conduction mechanisms.

On correcting the slope in region II for conduction mechanism I, it is found that the corrected slopes agree with measured work functions for all stages of activation (see Fig. 4).

The contribution of the pores to the total conductivity can be estimated in an elementary way: in any electron gas, in thermal equilibrium

in the absence of a field, the electrons have a mean velocity $\bar{v}$ in all directions. When a field F is applied, the electrons (of charge e and mass m) are subject to an acceleration a in the field direction during the time t which the electrons take to cover their mean free path ℓ.

$$a = \frac{eF}{m} \tag{15}$$

The mean increase in velocity $\overline{\Delta v}$ in the field direction during the time t is

$$\overline{\Delta v} = \frac{eF}{2m} t \tag{16}$$

If $\overline{\Delta v} << v$, which will be so for small fields across each pore (or generally so in solids), then

$$t = \frac{\ell}{\bar{v}} \tag{17}$$

and

$$\overline{\Delta v} = \frac{eF}{2m} \frac{\ell}{\bar{v}} \tag{18}$$

At the end of the mean free path, this increase in velocity is destroyed by collision. Therefore $\overline{\Delta v}$ represents the mean drift of the electrons in the field direction and therefore the current density,

$$i = \rho \overline{\Delta v} = \rho \frac{eF}{2m} \frac{\ell}{\bar{v}} \tag{19}$$

where ρ = mean space charge density in pore. Thus, for low fields (for which the above calculation is valid), Ohm's law is obeyed and

$$\sigma = \rho \frac{e\ell}{2m\bar{v}} \tag{20}$$

The space charge density ρ may immediately be related to the saturated emission current density I by way of elementary kinetic theory:

$$(1-r)\rho = I(2\pi m/kT)^{1/2} \qquad (21)$$

(Actually Vink and Loosjes performed a much more sophisticated calculation for ρ taking into account the potential maximum existing inside each pore due to space charge. The result is not appreciably different from eq. (21) in region II).

Combining (20) and (21),

$$\sigma = I(2\pi m/kT)^{1/2} \frac{e\ell}{2mv} \qquad (22)$$

Taking I = 10 amperes/cm^2 at 1000°K (pulsed value), $\ell = 2\mu$ ($\sim$ pore diameter), $\bar{v} = 2 \times 10^7$ cm/sec (thermal velocity), we find $\sigma = 2 \times 10^{-2}\ \Omega^{-1}\text{cm}^{-1}$. Observed values of σ at 1000°K for well-activated cathodes vary between 3×10^{-3} and 7×10^{-3} (latter is Vink's highest value). Hence calculated σ is sufficient as to order of magnitude to explain experimental results. Also note that $\sigma \sim$ I for small fields so that this explains why the corrected slope $\approx$ work function.

With respect to the curved i-V characteristics in region II, this is to be expected on the basis of the pore picture as may be crudely shown as follows.

Returning to (16), $\overline{\Delta v} = \frac{eF}{2m} t$

If $\bar{v} \ll \overline{\Delta v}$ (case of high fields in pore),

in limit

$$t = \frac{\ell}{\overline{\Delta v}} \qquad (23)$$

$$\bar{\Delta v} = \frac{eF}{2m}\frac{\ell}{\Delta V} \tag{24}$$

$$\bar{\Delta v} = \sqrt{\frac{eF}{2m}\,\ell} \tag{25}$$

$$i = \rho\sqrt{\frac{eF}{2m}\,\ell} \tag{26}$$

This accounts for the curved i-V characteristics in region II.

At higher temperature the more exact calculation of Vink and Loosjes including the effect of space charge gives rise to a potential maximum inside the pore which increases rapidly with T (Fig. 5). This makes the mean space charge density smaller than would be given by simple kinetic theory and in region III, σ^- lags behind the straight line characteristic of region II. Also, if the internal field gets more important than the applied field, t becomes independent of F and we return to (17) and (20). This may possibly explain the linearity in the i-V characteristics in region III.

Thus, Vink and Loosjes make out quite a convincing case for pore conduction in the cathodes studied by them (which were essentially commercial cathode ray gun type cathodes. The concept of dominant pore conduction at high temperatures has not yet been universally accepted, the main dissenters being Hannay, MacNair and White[8]. They have presented a number of arguments designed to show that pore conduction. while present, does not constitute the primary mechanism. Of these arguments, the following two are probably the most cogent:

1. Treatment with excess methane which deposits carbon over all surfaces (even making the interior of the cathode gray) kills the emission without materially affecting the conductivity at high temperature.

2. The calculated value of σ^- using eq. (22) (taking $\ell = 2.3\,\mu$ because of 1 atm. of He introduced to set an upper limit on ℓ) and the observed value of I for their cathode (20 ma/cm^2 at 1000°K) is 6×10^{-5} Ω^{-1} cm^{-1} whereas the observed value of σ^- for the same cathode was 5×10^{-4} Ω^{-1} cm^{-1}.

The reasons for the disparity in the data obtained by Vink and Loosjes on the one hand and by Hannay, MacNair and White on the other are not yet clear. It is to be noted, however, that the configuration and activation method employed by the latter group are both quite different from conventional commercial ones and that their cathode was thermionically far less active than well-activated commercial cathodes (20 ma/cm^2 vs. 10 amperes/cm^2).

Further theoretical interpretation, to be given below, will be based on the data of Vink and Loosjes.

One of the main consequences of the Vink-Loosjes model (see reference[10]) is that it is the slope of log σ^- vs. 1/T in region I which is related to an energy level diagram and not that in region II. Thus, $\Delta\varepsilon_d$ should be as low as 0.1 - 0.4 e.v. In this case strong ionization above 800°K occurs (for example, with $\Delta\varepsilon_d$ = 0.2 e.v. and T = 1000°K, $\frac{4N_b}{P} e^{\Delta\varepsilon_d/kT} = .08$) and if we stick to a simple semiconductor model, we are now dealing with case (b) -- i.e. eqs. (13) and (14). Note that now $\phi_{Rich} = \chi = 1$ e.v. The calculated value of $I_{1000°K} \cong 1$ amp/cm^2 compared to the experimental value of 10 amperes/cm^2, which represents not unreasonable agreement.

7. Evidence for p-type Conductivity

It is now necessary for completeness to mention recent data of Wright[11] and Morgulis and Iagovdik[12]. These data pertain to Hall measurements[11] and thermal e.m.f. measurements[12] from which one can obtain the sign of the carrier and with proper interpretation in simple cases, the density of charge carriers as well. Both groups of workers have reported p-type conductivity at lower temperatures reverting to n-type conductivity at higher temperatures.

These data unfortunately greatly complicate the picture and, moreover, these data have not yet been generally believed. Indeed Wright[11] has very recently retracted some of his previous conclusions by stating that the p-type conduction was "definitely foreign to the Ba-SrO system."

8. Latest Theory

A theory has just been advanced by du Pre, Hutner and Rittner[13] which attempts to incorporate into a single consistent picture a more complicated semiconductor model and the Vink-Loosjes picture so as to permit an explanation of many of the important observations on oxide cathodes, including the change in work function and conduction slope with activation. The theory includes the semiconductor model shown in Fig. 6 as well as the Vink-Loosjes picture of the pore conduction mechanism at higher temperatures. The semiconductor model comprises a full band, a conduction band (separation equal to 1.7 e.v.) donors 0.3 e.v. below the conduction band, acceptors 1 e.v. below the conduction band

and χ = 1 e.v. It is assumed for simplicity that there is a fixed density of acceptors in the cathode (due perhaps to lattice defects) and the classical interpretation of activation as a gradual increase in donor concentration is retained. As long as $N_d < N_a$, the cathode is poorly activated; when $N_d > N_a$, the cathode becomes well activated. The choice of values was effected as follows: the work function varies between 2 and 1 e.v. on activation. The lower value was taken as χ and the higher one as the energy separation between the acceptor levels and a point outside the cathode; the position of the donor level was chosen to give the required low slopes of Region I. The full band was taken to be 0.7 e.v. below the acceptor level in order to obtain the maximum slope observed by Vink in region I for poorly activated cathodes. This makes for a thermal band separation of only 1.7 e.v., compared to an optical separation of 3.8 e.v. Originally this was not considered a difficulty. Maximum N_d was taken from chemical data to be $3 \times 10^{17}/cm^3$, whereas minimum N_d (10^{17}) and fixed Na (1.5×10^{17}) were chosen by trial to give the best fit of the data. Both values are entirely reasonable as to order of magnitude.

The expression for the conductivity is

$$\sigma = n_e e b_e + n_h e b_h \qquad (27)$$

In the absence of data concerning the mobilities, we have taken

$$b_e = b_h$$

and have neglected the temperature dependence of these quantities, which is probably small compared to that of n_e and n_h.

Thus,

$$\sigma \sim (n_e + n_h) \quad ;$$

$$\rho \sim \frac{1}{n_e + n_h}$$

$$n_e = P e^{\zeta/kT}$$

and $$n_h = Q e^{(-\zeta/kT - \Delta E/kT)} \quad .$$

Thus knowledge of ζ permits an estimate of the specific resistance vs. activation and temperature. Similarly, because of the general emission equation

$$I = AT^2(1 - r)e^{-(\chi - \zeta)/kT} \quad ,$$

knowledge of ζ permits a calculation of the emission current density vs. activation and temperature.

The Fermi level was calculated numerically from eq. (9) for several values of N_d and for varying temperatures between 0 and 1100°K, and from this information σ and I were determined.

CONDUCTIVITY

Fig. 7 shows calculated values of $\log \left[10^{17}/(n_e + n_h) \right]$ plotted as a function of $10^4/T$ for different donor concentrations, and hence for different stages of activation. The graph indicates that the model presented here predicts decreasing slopes in region I with increasing activation, in agreement with Vink's experimental results. (See also Table I). In fact, low slopes occur for most stages of activation except the very poor ones, which is also in accord with Vink's data. (In concordance with

the Vink-Loosjes concept that the conductivity above about 800°K is primarily determined by conduction through the electron gas in the pores, the curves of Fig. 7 have not been extended above 800°K.)

Furthermore, the type of conductivity in region I can be either n- or p-type, as is indicated in Fig. 7 and in Table I; it is evident that the model predicts p-type conductivity for the more poorly activated cathodes. For these cathodes, however, the conductivity at higher temperatures may become n-type since in region II the effective cross section for the electron current increases enormously and in addition the mean mobility of the electrons becomes much greater than that of the holes. Thus, these cathodes may show a p-n transition at about the same temperature where the transition from region I to region II occurs. On the other hand, well-activated cathodes should always show n-type conductivity.

THERMIONIC EMISSION

The thermionic emission current was calculated, in the temperature range from 800° to 1100°K, from the general emission equation using the values of $\zeta(T)$ determined from eq. (9). These calculated currents were then used to make Richardson plots (log I/T^2 vs. $1/T$), and straight lines were obtained. Thus, the calculated values of the current can also be represented by

$$I = A_{Rich} T^2 \exp(-\phi_{Rich}/kT). \qquad (28)$$

The quantities, A_{Rich}, ϕ_{Rich}, and $I_{1000°K}$, as determined from these calculations for different stages of activation, i.e. for different

values of N_d, are shown in Table I. The magnitude of ϕ_{Rich} varies from 2.1 to 0.93 e.v. with increasing activation, in good agreement with experiment. Similarly, the corresponding values of A_{Rich} check reasonably well with observations, as may be seen from the calculated values of I at 1000°K. Moreover, a semilogarithmic plot of A_{Rich} vs. ϕ_{Rich} for different stages of activation is essentially a straight line (see Fig. 8) and in good agreement with Veenemans' data[14].

We wish to emphasize that since A_{Rich} and ϕ_{Rich} are constants independent of temperature,

$$\phi_{Rich} \neq \chi - \zeta(T) \quad , \tag{29}$$

and therefore

$$A_{Rich} \neq A$$

as may also be seen in Table I. Thus, the temperature independent work functions, ϕ_{Rich}, obtained from Richardson plots do not measure directly the energy difference between the Fermi level and a point just outside the cathode. On the other hand, there is a different technique for determining work functions, namely contact p.d. measurements. The ϕ c.p.d.'s so determined are temperature dependent and actually measure the position of the Fermi level, for according to theory,

$$\phi_{c.p.d.} = \chi - \zeta(T) \quad ;$$

and therefore

$$\phi_{c.p.d.} \neq \phi_{Rich}$$

A plot of the variation of the Fermi level with temperature is presented in Fig. 9. A comparison of the values of $\phi_{c.p.d.}$ as read from this figure for $N_d = 3 \times 10^{17}/cm^3$ with the two values of $\phi_{c.p.d.}$ measured by Huber[15] is shown at the bottom of Table I. The absolute magnitude of the calculated $\phi_{c.p.d.}$ and its temperature variation agree remarkably well with Huber's values, although the excellence of the agreement is, no doubt, fortuitous.

In Fig. 9 note that in the temperature range from 800°K to 1100°K, ζ (T) is closely approximated by a straight line and can be represented by the formula

$$\zeta = \zeta_o - \alpha kT \tag{30}$$

Inserting this in the general emission formula, we get

$$I = AT^2 \exp(-(\chi - \zeta_o + \alpha kT)/kT) = Ae^{-\alpha} T^2 \exp(-\chi - \zeta_o)/kT. \tag{31}$$

Thus

$$A_{Rich} = Ae^{-\alpha}$$

and

$$\phi_{Rich} = \chi - \zeta_o \tag{32}$$

This last equation clearly shows that ϕ_{Rich} may also be obtained by extrapolating linearly to 0°K the high temperature part of each ζ curve. Numerical confirmation of this statement is shown by a comparison of the extrapolated ϕ_{Rich} values in Fig. 9 with the results in column 5 of Table I. It may also be seen from Fig. 9 that whereas in a well-activated

cathode $\phi_{c.p.d.} > \phi_{Rich}$, the model predicts for a cathode, so poorly activated as to be p-type in region I, that $\phi_{c.p.d.} < \phi_{Rich}$.

At the same American Physical Society meeting at which this theory was first expressed publicly, Apker presented some results of his electron emission technique for BaO, showing that the Fermi level is about 3.7 e.v. above the full band at room temperature. Thus, unless one assumes the operation of a most unusual selection rule, our 1.7 e.v. gap would seem to be much too small. Since there is reason for preferring Apker's results to those of Wright or of Morgulis and Iagovdik the dilemma can be resolved by lowering the full band to a position 3.8 e.v. below the conduction band while keeping all other features of the model unchanged. Since the full band contribution was negligible anyway in all cases in the preceding calculation save in those cases dealing with p-type conduction, all of the previous results still stand except those dealing with p-type conduction. Thus, the combination of the ammended semiconductor model with the Vink-Loosjes concept of conduction by an electron gas in the pores appears to explain in a natural way many of the accepted experimental facts pertaining to conduction and thermionic emission of commercial (Ba-Sr)O cathodes.

9. References

1) de Boer, "Electron Emission and Adsorption Phenomena," Cambridge University Press (1935).

2) Blewett, J. App. Physics 10, 668, 831 (1939).

3) Eisenstein, "Advances in Electronics. I. Oxide Coated Cathodes," Academic Press, Inc., New York (1948).

4) Seitz, "Modern Theory of Solids," McGraw Hill Co., New York (1940).

5) Hutner, Rittner, du Pré, Philips Research Reports 5, 188 (1950).

6) Nishibori and Kawamura, Phys. Math. Soc. Japan Proc. 22, 378 (1940).

7) Bien, Technical Report No. 73, Research Lab. of Electronics, Mass. Inst. of Techn., June 1949.

8) Hannay, MacNair, and White, J. App. Phys. 20, 669 (1949).

9) Vink and Loosjes, Philips Research Reports 4, 449 (1949).

10) Rittner, du Pré and Hutner, Phys. Rev. 76, 996 (1949).

11) Wright, Nature 164, 714 (1949); British, J. App. Physics 1,150 (1950).

12) Morgulis and Bagovdik, Report of the USSR Academy of Science LIX, 247 (1948).

13) du Pré, Hutner, Rittner, Phys. Rev. 78, 567 (1950).

14) Veenemans, Ned., Tijdschr. Natuurk. 10, 1 (1943).

15) Huber, Thesis, Berlin (1941).

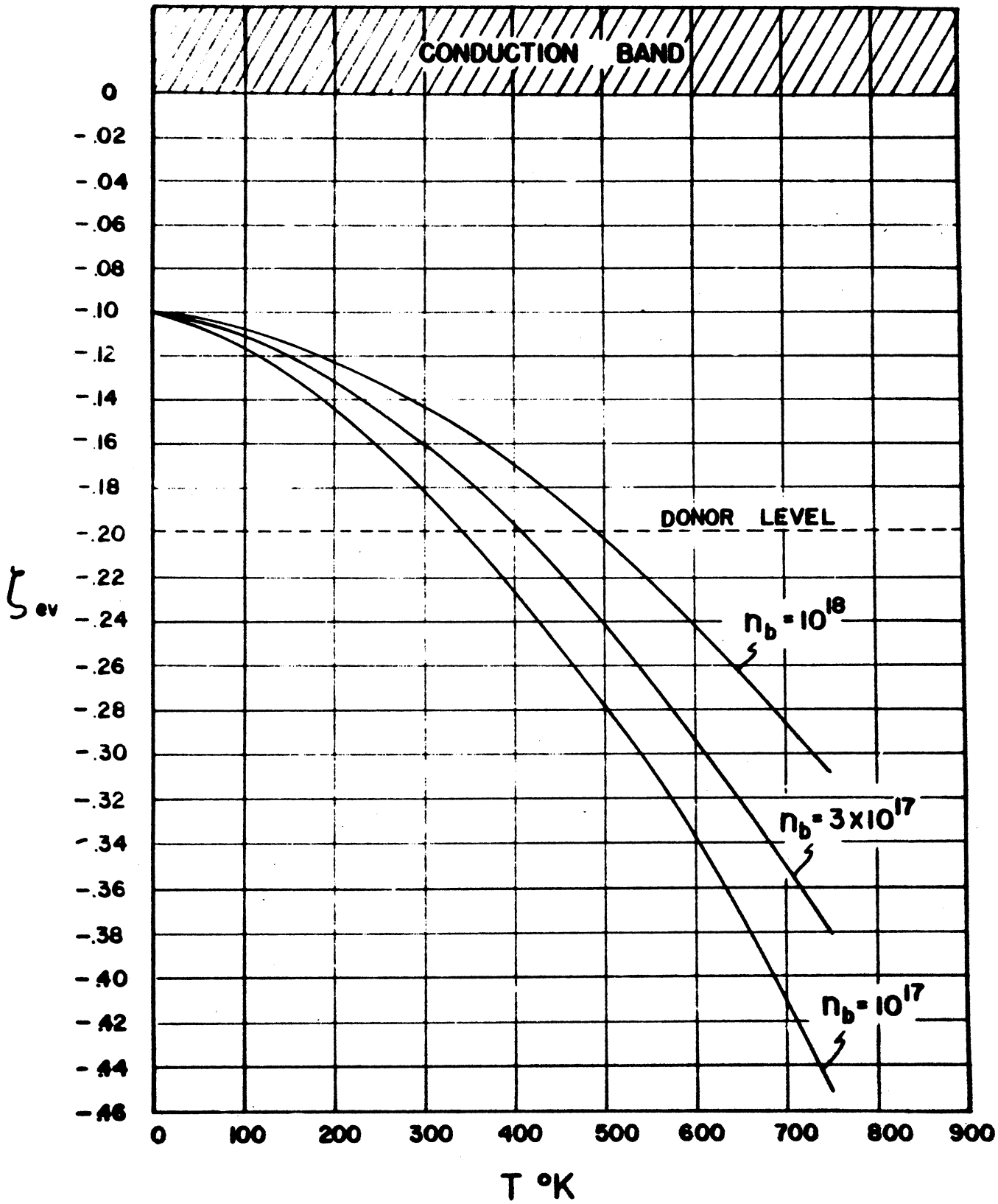

TEMPERATURE DEPENDENCE OF FERMI LEVEL
IN SIMPLE n-TYPE SEMICONDUCTOR

FIG. 1

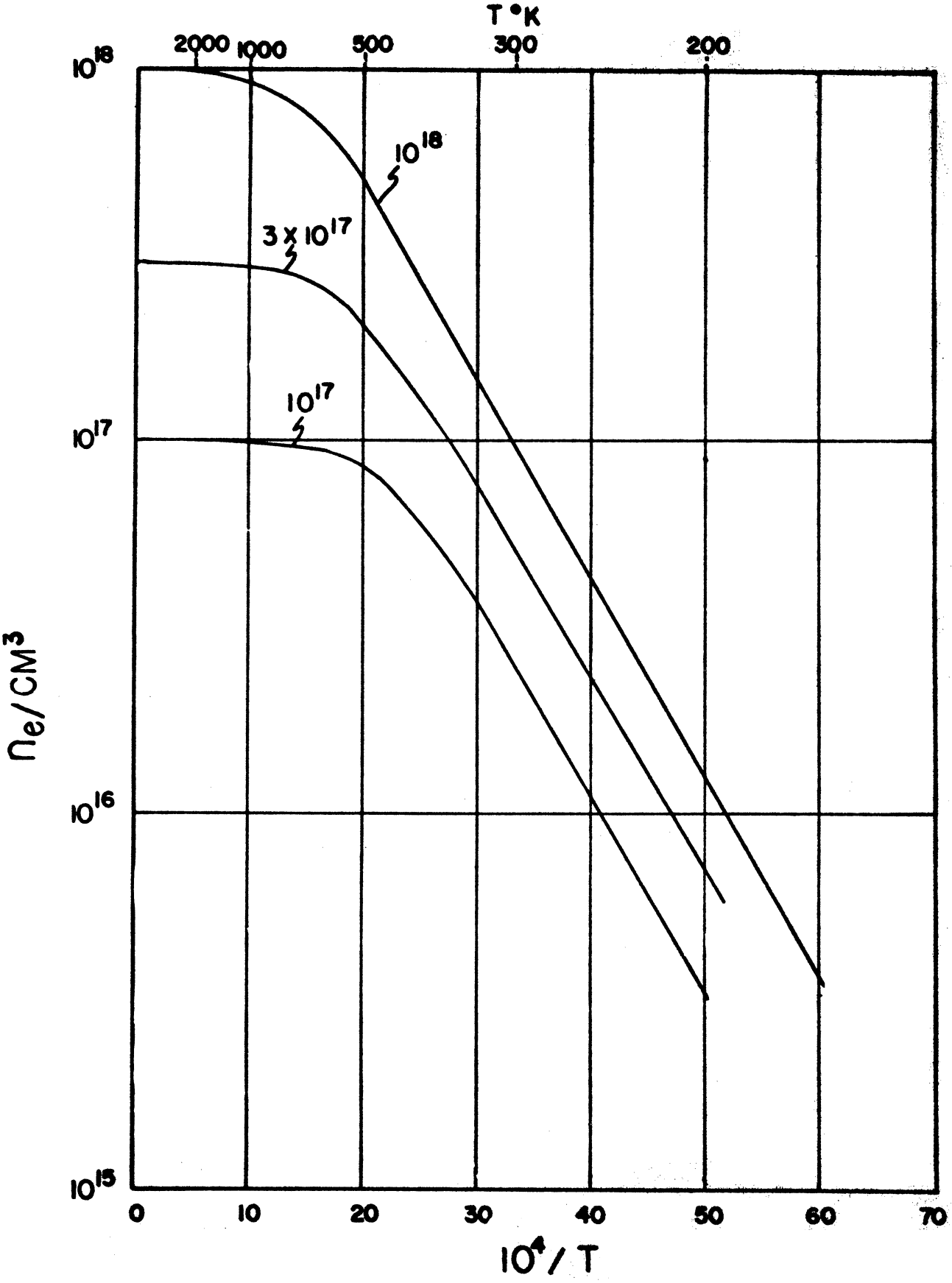

DENSITY OF FREE ELECTRONS IN SIMPLE n-TYPE SEMICONDUCTOR

FIG. 2

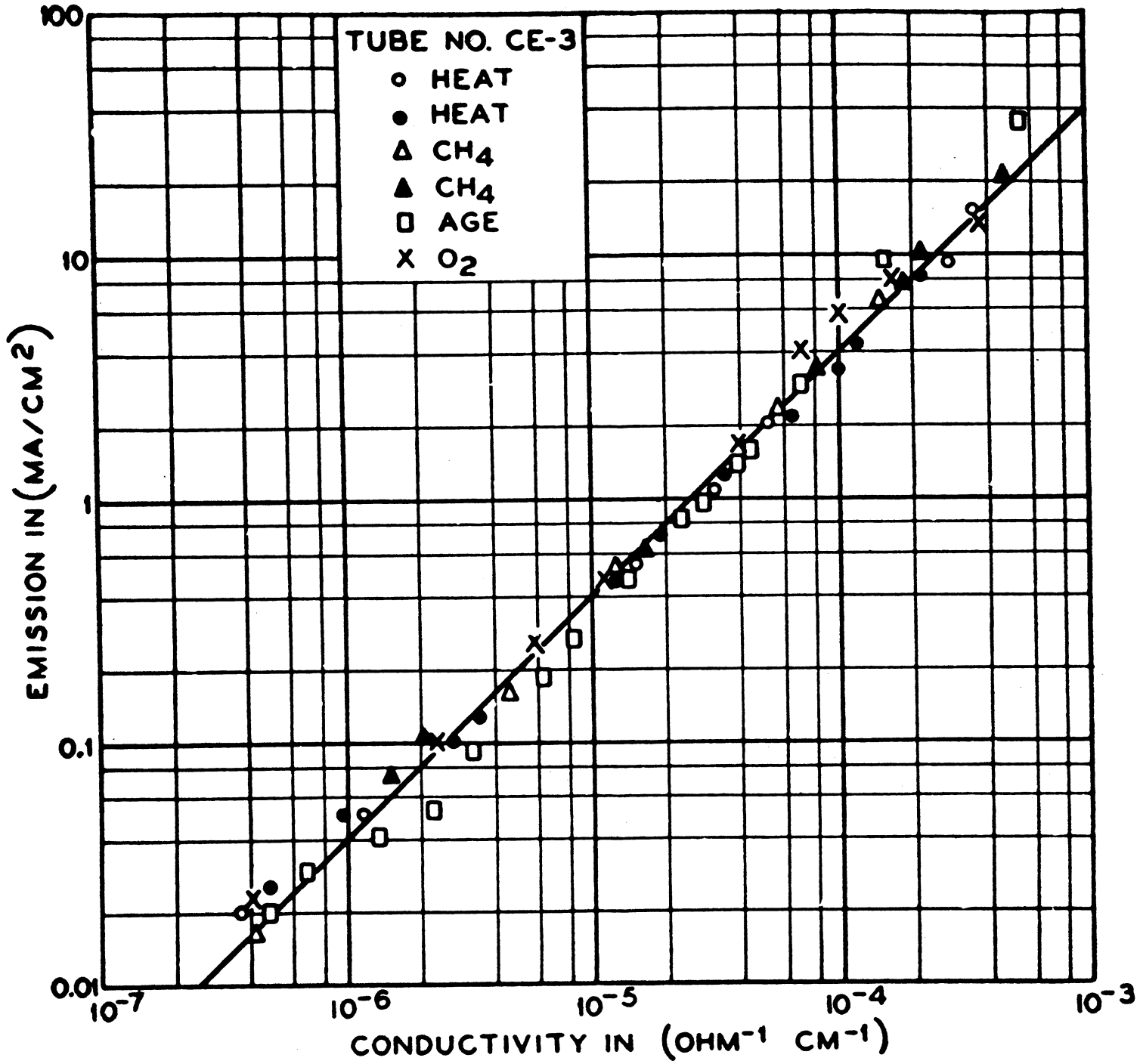

Conductivity and emission upon activation of the (Ba, Sr)O, for a typical tube.

FIG. 3

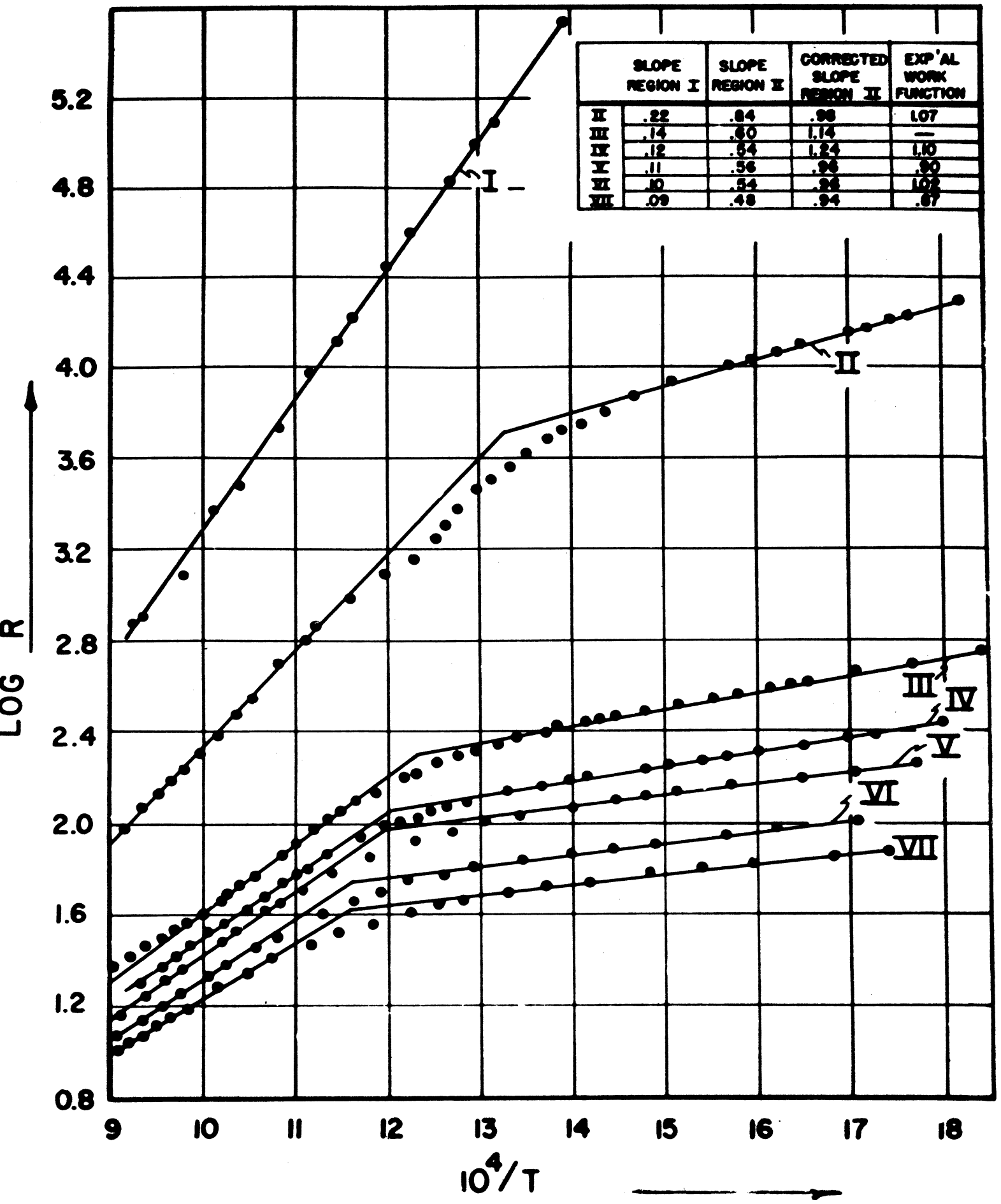
SLOPE REGION I
SLOPE REGION II
CORRECTED SLOPE REGION II
EXP'AL WORK FUNCTION
II .22 .84 .98 1.07
III .14 .60 1.14 —
IV .12 .54 1.24 1.10
V .11 .56 .98 .90
VI .10 .54 .98 1.02
VII .09 .48 .94 .87
I
II
III
IV
V
VI
VII
LOG R
5.2
4.8
4.4
4.0
3.6
3.2
2.8
2.4
2.0
1.6
1.2
0.8
9
10
11
12
13
14
15
16
17
18
10⁴/T

FIG. 4

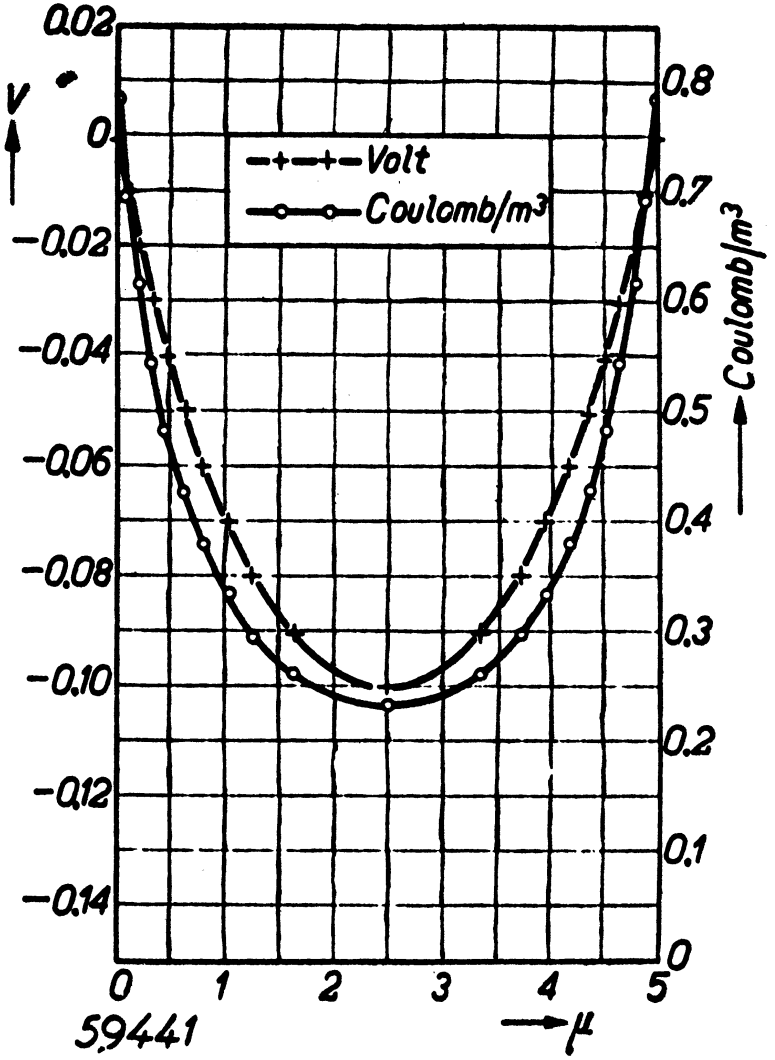

FIG. 5

The electron density and the potential between infinite flat emitting surfaces. $I_s = 3{\cdot}82.10^4$ A/m², $T = 952$ °K, distance $d = 5$ μ.

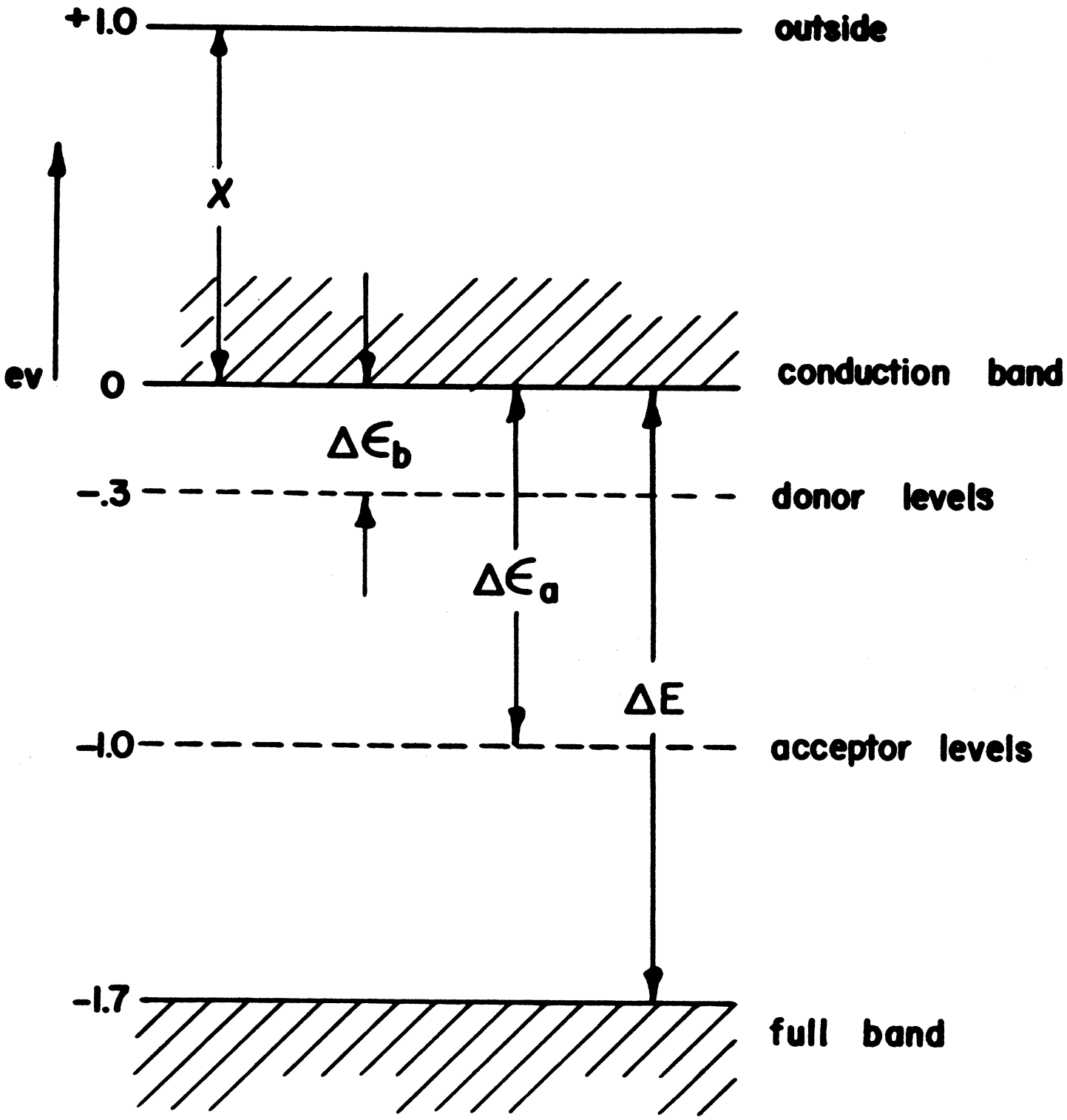
+1.0
outside
X
ev
0
conduction band
$\Delta\epsilon_b$
-.3
donor levels
$\Delta\epsilon_a$
ΔE
-1.0
acceptor levels
-1.7
full band

FIG. 6

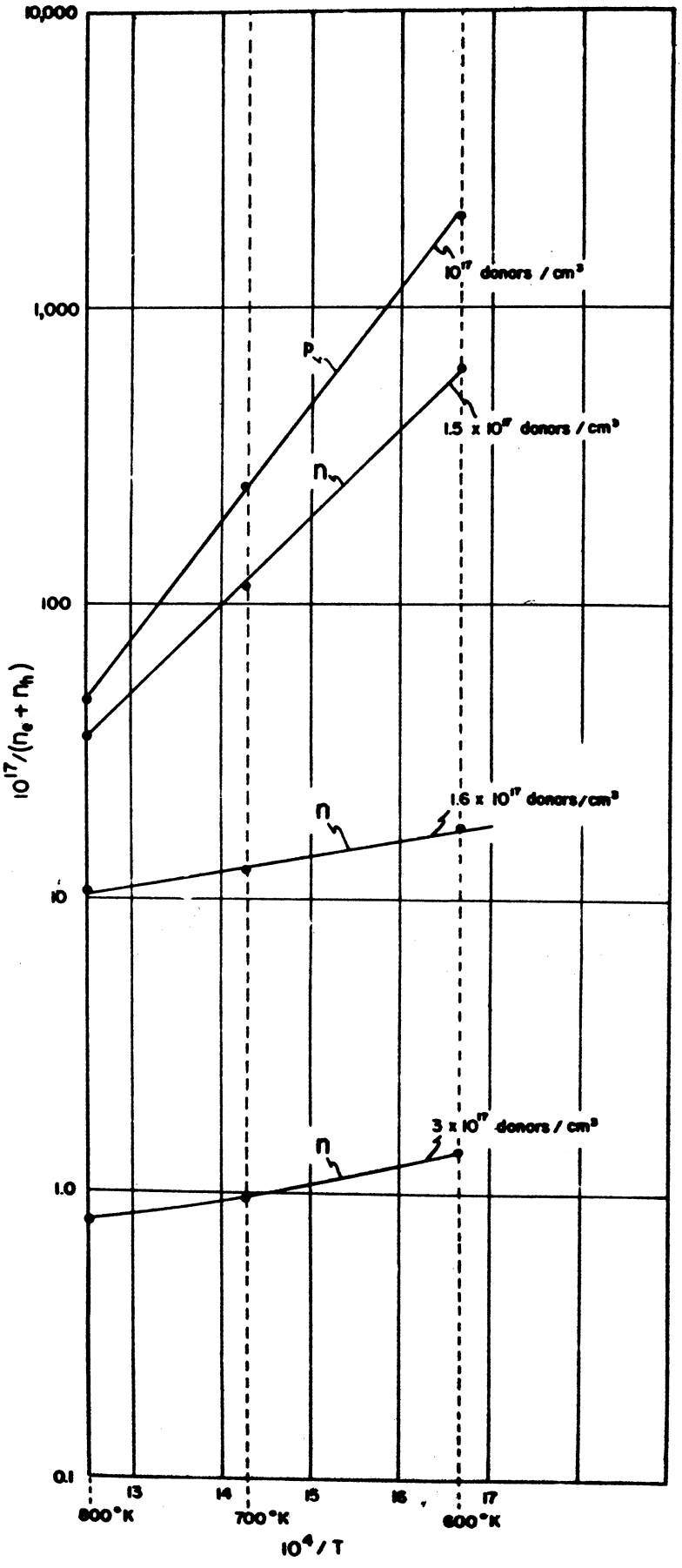
10,000
1,000
100
10
1.0
0.1
$10^{17}/(n_e + n_h)$
10^{17} donors / cm^3
p
1.5 x 10^{17} donors / cm^3
n
1.6 x 10^{17} donors/cm^3
n
3 x 10^{17} donors / cm^3
n
13
14
15
16
17
800°K
700°K
600°K
10^4 / T

FIG. 7

n_b	T	ζ (T)	$\phi_{c.p.d.} = (\chi - \zeta)$	ϕ_{Rich}	A_{Rich}	$i_{1000°K}$	Slope in Reg. I	Type of Conduction
$1 \times 10^{17}/cm^3$	600°K	-.97 ev	1.97 ev	ev	amps/cm^2	amps	ev	
	700	-.96	1.96				.76	p
	800	-.95	1.95					
	900	-.93	1.93	2.10	1,105.	.0288		
	1100	-.88	1.88					
1.5×10^{17}	600	-.67	1.67					
	700	-.70	1.70				.58	n
	800	-.73	1.73					
	900	-.76	1.76	1.50	4.18	.115		
	1100	-.81	1.81					
1.6×10^{17}	600	-.49	1.49					
	700	-.56	1.56				.11	n
	800	-.64	1.64					
	900	-.71	1.71	1.21	.211	.17		
	1100	-.80	1.80					
3×10^{17}	600	-.36	1.36					
	700	-.41	1.41				.12	n
	800	-.47	1.47					
	900	-.53	1.53	.93	.049	1.01		
	1100	-.67	1.67					

T	$\phi_{c.p.d.}$ (Huber)	$\phi_{c.p.d.}$ (Calculated)
770°K	1.46 ev	1.45 ev
640	1.38	1.38

TABLE I

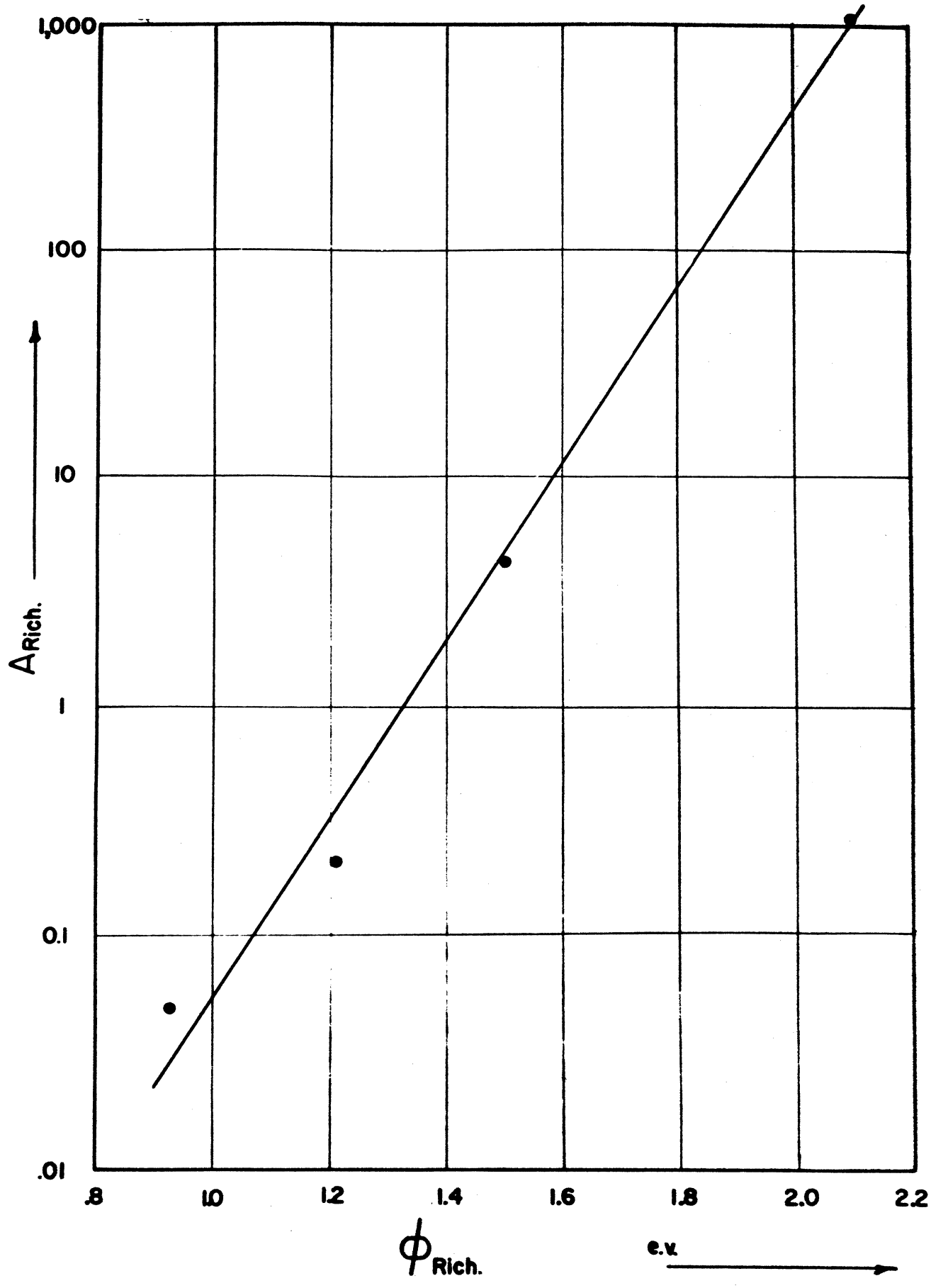

FIG. 8

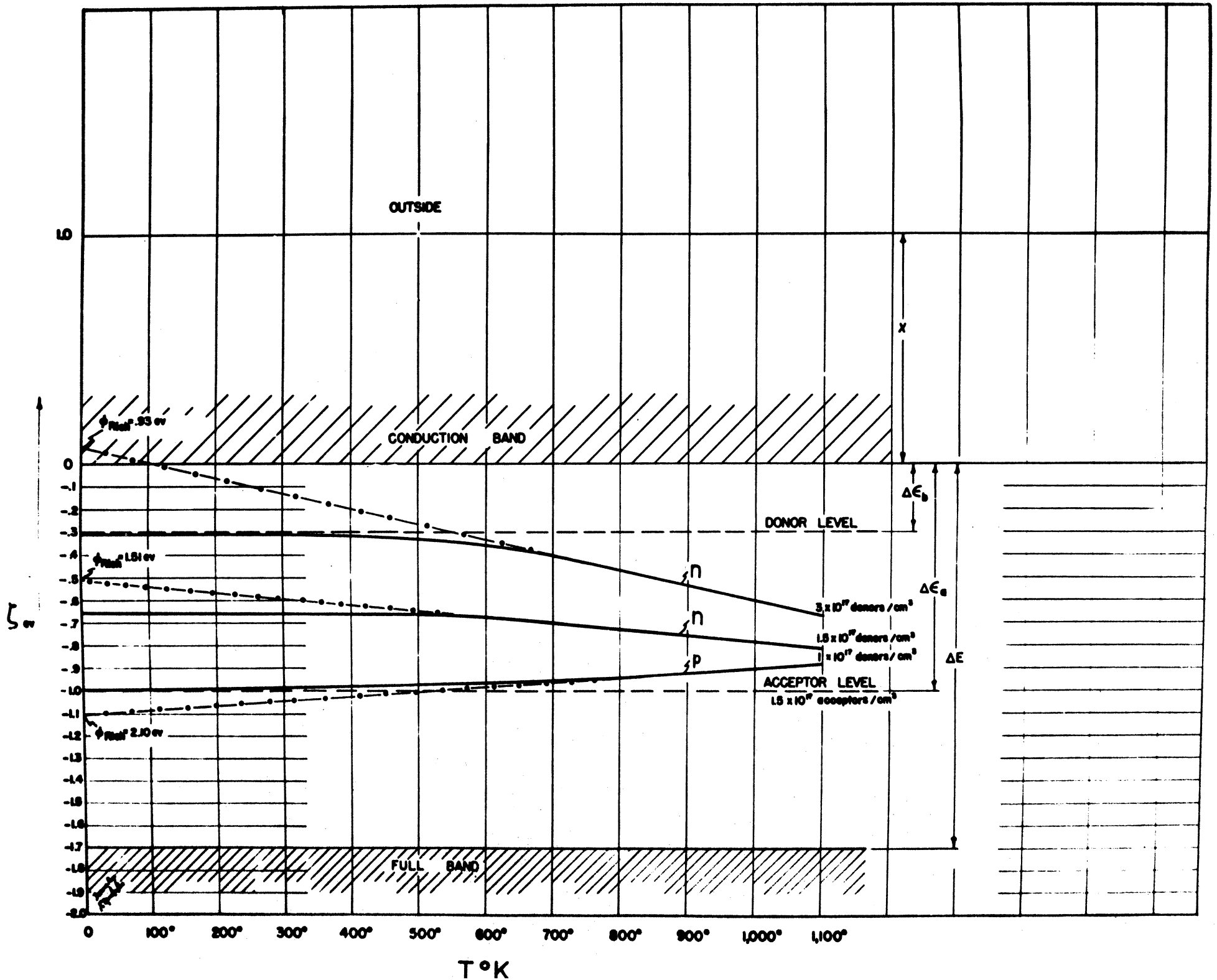
OUTSIDE
5
0
-.1
-.2
-.3
-.4
-.5
-.6
-.7
-.8
-.9
-1.0
-1.1
-1.2
-1.3
-1.4
-1.5
-1.6
-1.7
-1.8
-1.9
-2.0
ζ ev
CONDUCTION BAND
FULL BAND
DONOR LEVEL
ACCEPTOR LEVEL
1.5 x 10^17 acceptors / cm^3
3 x 10^17 donors / cm^3
1.5 x 10^17 donors / cm^3
1 x 10^17 donors / cm^3
n
n
p
χ
Δε_b
Δε_a
ΔE
0
100°
200°
300°
400°
500°
600°
700°
800°
900°
1,000°
1,100°
T °K

FIG. 9

II. PHOTOCONDUCTIVITY IN SEMICONDUCTORS

I. Introduction

Historically, the first discovery of a photoeffect in solids was made by W. Smith in 1873 who noted a change in the electrical resistance of metallic Se on illumination. The early commercial photocells consisted of thin films of "metallic" Se deposited over two interpenetrating electrodes. These cells in time were supplanted by photoemissive and photovoltaic cells which had certain important advantages in operating characteristics, notably improved linearity to light intensity and improved frequency response. In fact commercial photoconductive cells essentially disappeared from the scene until World War II when important improvements were made in photoconductive cells, improvements stimulated by military applications: secret signalling and passive detection of "thermal" bodies. These applications were made possible by the fact that the sensitivity of some photoconductive semiconductors, notably Tl_2S, PbS, PbSe, and PbTe extend appreciably into the infrared. Additional applications utilized since the war are the use of PbS cells for sound reproduction and astronomical detection and the use of all the Pb cells for infrared spectroscopy.

2. Expectations from Band Scheme

The phenomenon of photoconductivity is immediately to be expected on the basis of the band theory of solids. Absorption

radiation raises electrons from the full band to the conduction band, leaving behind positive holes. Both electrons and holes constitute free charge carriers which can contribute to an enhanced conductivity. The situation is similar for impurity semiconductors except that only one type of charge carrier is released and that the magnitude of the absorption is less. In fact the photoconductivity problem could be phrased: "Why are not all non-metallic substances photoconductive?" The answer to this question is that in most cases the charge carriers do not remain free for a sufficiently long period to materially increase the conductivity; they may disappear very rapidly into traps (which is the important process in insulators, such as crystal counters, not to be discussed here) or by recombination with each other or with an "ionized" impurity level (which is the important process in semiconductors). Before delving further into the theory, some of the important experimental facts about semiconductor photocells (Tl_2S, PbS, PbSe, PbTe) will first be recited.

3. Experimental Facts

Thallous Sulfide Cell

This cell was first discovered by Case in 1917 and was relatively recently developed into a radiation detector of extraordinary sensitivity by Cashman. Fig. 1 shows a typical cell and electrode structure. Pure Tl_2S is vacuum evaporated over the electrodes to a thickness of about $0.5\,\mu$. At this stage the photosensitivity is negligible.

Photosensitization is then effected by admitting O_2 at a low pressure and heating the layer to a few hundred degrees C. This process increases the dark resistance and the photoresponse (defined as $\Delta I/I_d$) and changes the conductivity from n- to p- type (see Fig. 2 and reference 1). Both the photocurrent (ΔI) and the dark current (I_d) are linear functions of the applied voltage. However, the photoresponse is non-linear with intensity of illumination (see Fig. 3). At very low levels of illumination with modulated light, the cells exhibit essentially a single time constant the value of which varies from cell to cell between 4×10^{-4} and 4×10^{-2} sec. at room temperature (see Fig. 4). An increase in temperature decreases the time constant greatly (in a particular case changing T from 27° to 75°C, produced a decrease in τ by a factor of 40), but this is obtained only at a sacrifice in photoresponse (which falls by a factor of 7 in the same range for that particular cell). The spectral response exhibits a cut off at 1.3 μ and a maximum at about 0.9 μ. (See Fig. 5.) The same data expressed as an apparent quantum yield show that many charge carriers may pass through the layer per incident quantum of radiation.

Lead Sulfide Cell

This cell is prepared usually in a similar manner to the Tl_2S cell but it can also be prepared by chemical deposition of a PbS mirror. Its characteristics are generally similar to those of Tl_2S cells. An interesting correlation has been found[6] between sensitivity and resistivity (see Fig. 6). Because of the lower intrinsic resistance, the

electrode arrangement is different from the Tl_2S case and provision is sometimes also made for cooling (see Fig. 7). Their spectral response extends considerably farther into the infrared with a cut-off at about 3.4 μ at room temperature, the cut-off wavelength extending further into the infrared with a decrease in temperature[2] (see Fig. 8). The dependence on illumination intensity has been found to be the same as that of Tl_2S cells in some cases and quite different (linear) in others (see Fig. 9).

Lead Selenide and Telluride Cells

These can be made in a manner similar to that described above or by sensitization with the electronegative constituent. The latter type of preparation has been developed by Simpson[3], particularly for PbTe cells. It is necessary to cool the cells to observe appreciable sensitivity. The spectral response is similar in both cases and extends out to about 6 μ at low temperatures (see Fig. 10). Again the threshold shifts to longer wavelengths on cooling[2].

4. Energy Level Diagram

In the case of PbS a careful study of the conduction mechanism has been made by Hintenberger[4] leading to the following conclusions. Heating a thin layer of PbS in vacuo causes slight removal of sulfur producing an n-type semiconductor. Heating in sulfur vapor produces a p-type semiconductor. The presumed stoichiometric composition shows a minimum in conductivity, but the substance is still in the class of semiconductors.

From the slope of the conductivity vs. 1/T data at low temperatures, it appears that the impurity levels are extremely close to their respective bands. Thus, the energy level diagram applying to this case is

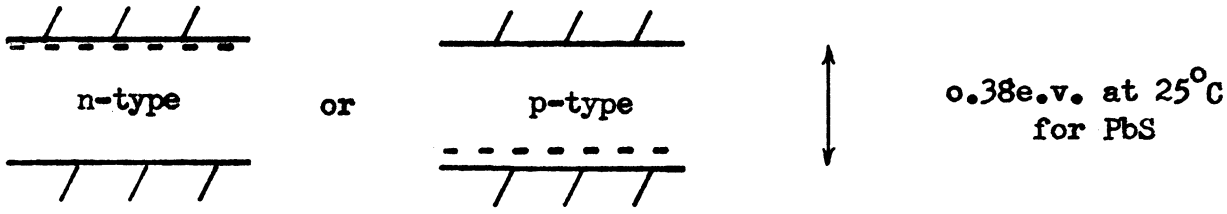

From the electrical properties, there is reason for believing that a similar diagram applies to the other substances as well, the band separation decreasing in the order: Tl_2S, PbS, $\left\{\begin{matrix}\text{PbSe} \\ \text{PbTe}\end{matrix}\right.$. Further support for this kind of diagram in all cases is found in the optical absorption coefficients measured in the region where the cells are sensitive. In all cases the absorption coefficients are of the order of 10^4 to 10^5 cm^{-1} which is so high as to imply that all the atoms of the material participate in the absorption process and not just the impurity atoms. These data also imply that the photoconductivity is associated with optical transitions from the full band to the conduction band and not from one impurity level to a band (or vice versa).

5. Photoconductivity Theory for Unsensitized Material

Let us now attempt to see why the semiconductor, before photosensitization, is not appreciably photoconductive. We shall consider only an n-type semiconductor: the argument is analogous for a p-type

semiconductor. For simplicity we shall make the following assumptions (a) complete ionization of donors (which is reasonable in view of the closeness of the donors to the conduction band); (b) the layer is so thin that the intensity of light is not a function of depth within the layer.

The density of free electrons in the dark at temperature T, we designate n_{e_d}; because of assumption (a) $n_{e_d} = N_d$. The density of holes, n_{h_d}, will be small compared to n_{e_d} because of the general relation:

$$n_{e_d} n_{h_d} = Pe^{\zeta/kT} Qe^{(-\zeta/kT - \Delta E/kT)} = PQe^{-\Delta E/kT} = \text{constant} \qquad (1)$$

For Tl_2S at room temperature, $n_{e_d} n_{h_d} \cong 10^{22}$.
If $N_d \sim 10^{18}/cm^3$ (a reasonable impurity content), $n_{h_d} \cong 10^4/cm^3$.

The small free hole density n_{h_d} is maintained in the dark kinetically by continuous thermal ionization and recombination. In equilibrium the rates of formation and recombination are equal. The latter rate will be given by the bimolecular recombination law

$$\left(\frac{dn_{h_d}}{dt}\right)_{form.} = \left(\frac{dn_{h_d}}{dt}\right)_{recomb.} = Bn_{e_d} n_{h_d} = BN_d n_{h_d} \qquad (2)$$

where B is the recombination probability. Under steady illumination with intensity J, the rate of formation of holes (and electrons) increases by an amount cJ, where c = number of charge carrier pairs created per second per unit volume under unit illumination. In the steady state the rates of formation and recombination are equal:

$$Bn_h n_e = BN_d n_{h_d} + cJ \qquad (3)$$

where n_h and n_e are the new equilibrium concentrations under conditions of illumination.

Since $\Delta n_e << N_d$, as will be proved in a moment,

$$n_e \cong N_d$$

Therefore,

$$BN_d(n_h - n_{h_d}) = cJ$$

$$\Delta n_h = \frac{cJ}{BN_d} = \Delta n_e \tag{4}$$

as the light creates electrons and holes in equal numbers.

The photosensitivity, expressed as $\Delta I/I_d$, is then

$$\frac{\Delta I}{I_d} = \frac{\Delta n_h e v_{h_\ell} + \Delta n_e e v_{e_\ell}}{n_{h_d} e v_{h_d} + n_{e_d} e v_{e_d}} \tag{5}$$

Since the optically released charges lose their extra velocity very rapidly ($<10^{-11}$ sec. for example $\{100$ mean free paths $\approx 10^{-4}$ cm traversed at rate of 10^7 cm/sec $\}$) by interaction with the lattice, for practically all of their lifetime the drift velocity of photo-released carriers will be identical with that of the thermally released carriers, i.e. $v_\ell = v_d$. Since this is only an order of magnitude calculation, we shall take $v_e = v_h$. Also, since $n_{h_d} << n_{e_d} = N_d$ and $\Delta n_e = \Delta n_h$,

$$\frac{\Delta I}{I_d} = \frac{2cJ}{BN_d^2} \tag{6}$$

The constant c may be readily calculated from the number of effective quanta/sec absorbed in a layer of thickness δ

$$c = \frac{fP}{h\gamma\delta} = \frac{5.095 \times 10^{12} \lambda_{/\mu} fP}{\delta cm} \quad \text{for J in } /\mu \text{ watts/cm}^2$$

where f = fraction of the incident radiation that is absorbed and P = efficiency factor for the creation of charge carrier pairs. For example for Tl_2S, $f \cong 0.75$, $\lambda_\mu \cong 0.9\mu$, $\delta \cong 5 \times 10^{-5}$ cm and assuming P = 1,

$$c \cong 6 \times 10^{16} \text{ cm}^{-3} \text{ sec}^{-1} \mu \text{ watt}^{-1} \text{ cm}^2$$

The recombination probability B is much more difficult to estimate but it is possible to determine an upper limit by assuming that every collision between a hole and an electron leads to recombination. In that case

$$B_{max} = Av \qquad (8)$$

where A is the collision cross-section and v the thermal velocity of the carriers. A may be estimated to be of atomic dimensions, i.e. $\sim 10^{-15}$ cm^2 and v = 10^7 cm/sec at 25°C. Hence $B_{max} \cong 10^{-8}$ cm^3 sec^{-1}. B will tend to be less than B_{max} because in the course of recombination energy must be given up to the lattice and this is usually not readily accomplished because the probability of the lattice accepting the excess energy as a large number of small vibrational quanta is very small. (In bulk Ge, experiments indicate that $B/B_{max} \cong 10^{-4}$.) The situation is different, however, for the non-symmetrical situation prevailing at surfaces as the excess energy can be imparted to the solid as a whole and therefore in a thin photocell layer B_{max} may possibly not exceed B by a great deal.

Using the above values of B_{max} and c, and for a reasonably high intensity of illumination (J = 1000μ watts/cm^2) and a value of $N_d = 10^{18}$/cm^3,

$$\frac{\Delta I}{I_d} = \frac{2 \times 6 \times 10^{16} \times 10^3}{10^{-8}\ (10^{18})^2} = 10^{-8}$$

(compared to experimental value of say 25

Note that

$$\Delta n_e = \frac{cJ}{BN} \cong 10^{10} \text{ is } << N_d \quad ,$$

one of the original assumptions, now proven. Even if the above calculation underestimated the photoresponse by several orders of magnitude, it is clear that an intrinsic semiconductor with appreciable impurity content will possess a negligible photosensitivity owing to the recombination of the optically released charges with the high density of thermally released charges.

It is also of some interest to estimate the time constant for the recombination process. This may be done as follows:

$$\frac{dn_h}{dt} = BN_d\ (n_{h_d} - n_h) = - BN_d \Delta n_h \qquad (9)$$

(a differential equation expressing the rate of disappearance of charge in a transient state).

Since

$$\Delta n_h = n_h - n_{h_d} \quad ;$$

$$\frac{d(\Delta n_h)}{dt} = \frac{dn_h}{dt}$$

Hence, the rate of disappearance with time of the excess holes produced by light will be

$$\frac{d(\Delta n_h)}{dt} = - BN_d \Delta n_h$$

Integrating,

$$\ell n \Delta n_h = \ell n (\Delta n_h)_{t=0} - BN_d t$$

or

$$\Delta n_h = (\Delta n_h)_{t=0} e^{-BN_d t} \tag{11}$$

an exponential decay with a time constant

$$\tau = \frac{1}{BN_d} \tag{12}$$

Using the above mentioned values,

$$\tau = 10^{-10} \text{ sec.}$$

again showing that the recombination proceeds so quickly that the average lifetime of the photoreleased carriers is negligibly small.

6. Photoconductivity Theory for Intrinsic Semiconductor Produced by Compensation of Impurities

It is clear from the above argument that in order to improve the photosensitivity, it is desirable to reduce the impurity content. Although it is possible to remove foreign impurities from materials to an extent of a few orders of magnitude better than $N_d = 10^{18}/cm^3$, discussed above, stoichiometric deviations are unavoidable. In most cases chemically undetectable quantities of such "impurities" may destroy the photosensitivity.

One might imagine that the introduction of oxygen is simply a trick for effectively removing the deleterious influence of the impurities. If into an n-type layer (produced by vacuum evaporation), p-type impurities (due say to O_2) are introduced in exactly equivalent amount, the result is

to convert the material into essentially an intrinsic semiconductor, either by direct recombination or by virtue of the fact that the electrons fall spontaneously from the donors (which were near the conduction band) to the acceptors (which are close to the full band). In this instance the thermal charge density, which is so important for the recombination process, is reduced to its minimum value for the chemical system under consideration; i.e., the intrinsic value of $n_{ed} = n_{hd}$.

It is therefore of interest to consider the problem of photosensitivity in an intrinsic semiconductor in much the same manner as that employed above. Again for simplicity we assume a very thin layer such that J is taken independent of depth. In the dark the density of electrons n_{ed} = density of holes $n_{hd} = n_d$. In the steady state with an illumination J, the recombination rate will be equal to the formation rate, i.e.

$$Bn^2 = Bn_d^2 + cJ \tag{13}$$

where n = equilibrium density of electrons and holes under illumination.

$$n = \sqrt{n_d^2 + \frac{c}{B} J}$$

$$n - n_d = \Delta n = -n_d + \sqrt{n_d^2 + \frac{c}{B} J}$$

$$\frac{\Delta n}{n_d} = -1 + \sqrt{1 + \frac{cJ}{Bn_d^2}} = \frac{\Delta I}{I_d} \tag{14}$$

Eq. (14) is precisely of the form observed experimentally in all Tl_2S cells and in many PbS and PbTe cells. Moreover, we may again estimate the constant involved, $\frac{c}{Bn_d^2}$.

It will be recalled (eq. (1)) that in general

$$n_{e_d} n_{h_d} = PQe^{-\Delta E/kT}$$

For an intrinsic semiconductor,

$$n_{e_d} = n_{h_d} = n_d = \sqrt{PQ}\, e^{-\Delta E/2kT} \tag{15}$$

For Tl_2S at room temperature,

$$n_d = 3 \times 10^{11}/cm^3$$

Hence taking c again = 6×10^{16}, B = $B_{max} \approx 10^{-8}$ and the above value of n_d, we find that

$$\frac{c}{Bn_d^2} = \frac{6 \times 10^{16}}{10^{-8} \times 9 \times 10^{22}} = 70 \quad ,$$

which is to be compared to experimental values of the order of 5. In view of the crude approximations employed in the calculation (particularly J independent of depth), this is to be construed as reasonable agreement between theory and experiment.

We could in the same manner as before compute the time constant for the recombination process from the differential equation expressing the rate of disappearance of charge

$$\frac{dn}{dt} = B(n_d^2 - n^2) \tag{16}$$

The detailed calculation (to be found in von Hippel and Rittner[5]) is much more complicated in this instance, but for the case of very low illumination level, the resulting expression for the time constant is substantially the

same as before:

$$\tau = \frac{1}{2\,B n_d} \approx 2 \times 10^{-4} \text{ sec.} \qquad (17)$$

The order of magnitude of τ is not unreasonable in view of the uncertainty in B and furthermore eq. (17) shows immediately why τ decreases with increasing T, as

$$n_d = \sqrt{PQ}\, e^{-\Delta E/2kT}$$

It is also easy to see why in this picture the apparent quantum yield can exceed 1. Each incident quantum creates on the average fP free charge carrier pairs. During their average lifetime, τ, the conductivity is enhanced such that $\frac{\tau\, b\, F}{d}$ extra charge carriers can flow through the material, where b = mobility, F = field-strength and d = electrode separation. Thus, the apparent quantum yield,

$$\eta = \frac{f\, P\, \tau\, b\, F}{d} \qquad (18)$$

It can also be shown that (18) is consistent with (14).

Taking f = 0.75 again, P = 1, $\tau = 4 \times 10^{-3}$ (average experimental value), b = 1 cm/sec/volt/cm, F = 500 volts/cm d = .1 cm, we find $\eta = 15$, in good agreement with experiment.

Note that this picture also explains the observations that heating in O_2 increases the dark resistance and the photoresponse, that the type of conductivity changes from n- to p- type (due to some excess O_2), and that the photocurrents and dark current are linear functions of the applied voltage.

In short the picture of a uniform "intrinsic" semiconductor produced by detailed balancing of n- and p- type impurities seems to have great success in accounting for the presently known properties of Tl_2S photocells. A picture of essentially this type, but in less refined form, was proposed by von Hippel and Rittner[5] several years ago for the case of Tl_2S.

7. n-p Barrier Picture

Quite a different explanation for the properties of PbS cells has been advanced by Sosnowski, Starkiewicz, and Simpson[6], who have proposed that part of the grains of the layer are n-type whereas the remainder are p-type. The inter-crystalline contacts between the two different types of grain are considered to constitute the controlling influence in the resistance. The picture of barriers between n-p contacts has been further developed by James[9], who has stressed that a homogeneous semiconductor produced by careful balance between n- and p- impurities will become split up into a large number of tiny n- and p- type regions owing to random fluctuations in impurity concentrations. We shall not discuss here the details of the pictures proposed by Sosnowski et al and by James; a detailed discussion of n-p contacts will, however, be included in the more general theory to be presented below.

The most direct experimental evidence for the presence of n-p barriers is twofold: a) on scanning a PbS layer with a small spot of light, photo-e.m.f.'s are observed which vary in sign and magnitude from point to point in the layer (see Fig. 11) (Sosnowski, Soole, Starkiewicz[7]); (b) from measurements of impedance vs. frequency, it is found that the

parallel resistance decreases with frequency, ostensibly due to the capacitative shunting of the barriers (Fig. 12) (Chasmar[8]).

8. General Theory

The method of preparation and properties of Tl_2S, PbS, PbSe, and PbTe photocells are so similar as to suggest that a single explanation should apply to this class of materials. It is apparent that the two pictures that have been proposed: a) intrinsic semiconductor, and (b) n-p barriers, are mutually exclusive and in fact as a general explanation of photoconductivity in semiconductors, each is subject to difficulties. The first picture fails to explain the two experiments on PbS cells just discussed and also carries the extremely stringent requirement that n- and p- type impurities balance each other so exactly that the maximum net impurity concentration anywhere in the layer be less than the intrinsic density of charge carriers (10^{16} in PbS and $10^{11}/cm^3$ in Tl_2S at 300°K). The second picture will not account for the bimolecular recombination law that has been observed in Tl_2S, PbS and PbTe photocells. A more general explanation has recently been advanced by Rittner[10], an explanation which follows naturally from one method of preparing the photocells and which reduces in limiting cases to essentially pictures (a) and (b) while avoiding the difficulty of the exact balancing of impurities.

It is perhaps not unreasonable to assume that the following events occur in the course of fabricating photocells by vacuum evaporation and subsequent sensitization. During vacuum evaporation of the material

to form a thin layer, a slight loss of the electronegative constituent occurs, giving rise to an n-type semiconductor in which the photosensitivity is extremely small owing to the rapid recombination of the electrons and holes created optically with the thermally produced charges. Subsequent heat treatment in the presence of the electronegative constituent or oxygen converts portions of the surfaces of the grains into p-type material thus calling into existence randomly distributed local n-p transition regions. As the "oxidation" proceeds further, the n-type conducting paths become more and more disrupted by the p-type regions until a point is reached where all charge carriers travelling between electrodes have to pass through some of the n-p transition regions. With still further "oxidation," continuous threads of p-type material of negligible photosensitivity are formed and these grow progressively thicker, until in the limit the layer may become completely p-type.

The properties of the photocell layer are determined mainly by those of the transition region which in turn depend upon the details of the impurity distribution. Fig. 13 illustrates the sort of impurity distribution to be anticipated in the sensitization process outlined above, i.e. the interpenetration of an n-type region of relatively constant donor concentration with a p-type region in which the acceptor concentration tails off with distance. To the left of line 1 in Fig. 13 some of the electrons from the donors fall spontaneously into the acceptors, completely filling the latter*. Since the net donor concentration remains high, the material is n-type. To the right of line 2 all of the donors are emptied of electrons by spontaneous transitions to the acceptors,* but since the net

*An alternative possibility, having essentially the same consequences, is the mutual annihilation of donors and acceptors by recombination.

acceptor concentration is high, the material is p-type. Between lines 1 and 2, the net impurity concentration is either zero or extremely small, and this transition region behaves essentially as an intrinsic semiconductor. The thickness of this quasi-intrinsic region increases with temperature because of the tendency of the Fermi level to merge with the intrinsic line at high temperatures (see Fig. 14). It is also larger the more gradually the concentration of p-type impurity varies with distance in the transition region. Thus, in general, a quasi-intrinsic region is to be expected, the thickness of which may vary widely depending upon the chemical and heat treatments employed and upon the operating temperature of the photocell. Moreover, the equilibrium condition that the Fermi level be everywhere the same requires transfer of electrons from the n-type region to the intrinsic region and from the intrinsic region to the p-type region. Thus, space charges are set up which correspond to potential barriers for the passage of charge carriers. The situation is illustrated by the energy level diagrams of Figs. 15 and 16 which show two limiting cases, one where the thickness of the quasi-intrinsic region is zero (a) (Fig. 15), and one where it is large (b) (Fig. 16), compared to the thickness of the space charge region. Although intermediate cases are of great interest we shall for simplicity discuss only these limiting ones.

Case (a) - Sharp n-p Transition (Fig. 15)

In a perfectly sharp contact between n- and p- type regions, the establishment of equilibrium requires that electrons be transferred from the n- to the p- type material in the neighborhood of the contact. This

creates a positive space charge in the n-type region and a negative space charge in the p-type region, corresponding to a variation of potential which, in the present instance, is continuous across the plane of contact and which obeys Poisson's equation in both regions. The height of the (rectifying) potential barrier so created is equal to the difference in the Fermi level positions which would obtain if the n- and p- type regions were separated. This height can vary from zero (high temperatures, low impurity content) to about the energy separation between the bands (low temperatures, high impurity content) as may be seen from the calculated values of the Fermi level for PbS (Fig. 14). With reasonable impurity content (ca 10^{17} - $10^{19}/cm^3$) the resistance of such a potential barrier can greatly exceed the resistance of an impurity semiconductor of comparable thickness.

On exposure to steady illumination, electrons are excited from the full band to the conduction band everywhere throughout the material. In both the n- and p- type regions far from the plane of contact, the electrons and positive holes created optically disappear so rapidly by recombination with the thermally produced charges that the net increase in charge carrier density is extremely small. However, electrons and holes produced in the space charge region are rapidly separated by the strong electric field; electrons are drawn into the n-type region and partially neutralize the positive space charge, whereas the holes are drawn into the p-type region and partially neutralize the negative space charge. Consequently, the height of the space charge barrier and the corresponding D.C. resistance are lowered. It will be noted that for each pair of charge carriers created optically and separated in the space charge

region (photovoltaic effect) many charge carrier pairs can pass over the barrier (photoconductive effect). On removing the illumination, the system will spontaneously return to its equilibrium state in the dark with great rapidity by thermionic emission over the barrier of the excess charge.

The following behavior is expected of a photocell which may be approximated by a large number of sharp barriers of the type just described shunted by thin well-conducting threads of n- or p- type material. The D.C. resistance will appear to be ohmic and will be determined at high temperatures by the barriers and at low temperatures by the thin conducting threads. The D.C. resistance will be considerably higner than the A.C. resistance at high frequencies; the former will be appreciably lowered by radiation but not the latter. The photoconductivity can be shown to be a linear function of the intensity of radiation up to very high levels for diode theory. The response time will probably be determined by the product of resistance and capacitance of the photocell.

Case (b) - Gradual n-p Transition (Fig. 16)

If the quasi-intrinsic region is much thicker than the space charge region, the potential barrier becomes split into two halves. Electrons and holes need only surmount the smaller barriers in order to recombine with each other. Under these circumstances the barrier resistances may be negligible with respect to the resistance of the quasi-intrinsic region in which case the properties of the latter will dominate The theory then reduces to that given above for an intrinsic semiconductor.

The following behavior is expected of a photocell which may be approximated by a large number of diffuse barriers of this type, shunted by thin threads of well-conducting material. The D.C. resistance and A.C. resistance at high frequencies will be the same and both will be equally affected by radiation. The resistance-temperature behavior will be similar to that of a homogeneous intrinsic semiconductor containing impurities. The photoconductivity will be a non-linear function of the intensity of radiation, following the bimolecular recombination law. The response time will be determined by either the recombination relaxation time or by the RC time constant, whichever is the longer.

The preceding discussion has stressed the extreme differences in properties resulting in two limiting cases. Obviously all shades of intermediate behavior are possible in actual photocells, for example, appreciable barrier contribution to the D.C. resistance and non-linearity with radiation intensity. There is evidence (linearity with J, A.C. measurements of Chasmar) that some of the PbS cells which have been studied may approximate the sharp transition case. On the other hand, the non-linear response to radiation which has been observed in Tl_2S and in other PbS and PbTe cells indicates more gradual n-p transitions in these layers.

Independently of the thickness of the quasi-intrinsic region, the general picture outlined above is capable of explaining a number of additional observations which have been mentioned previously, for example, the sensitizing role of oxygen or of the electronegative constituent, the requirement for high photosensitivity that both n- and p- type impurities be present simultaneously, the change in sign of the thermal

e.m.f. coefficient with "oxidation," the correlation of maximum photosensitivity (expressed as $\Delta I/I_d$) with minimum conductivity, increase in photosensitivity with a decrease in temperature, quantum yields exceeding unity and the occurence of photo-e.m.f.'s varying in magnitude and sign from point to point in the layer.

9. References

1) von Hippel et al, J. Chem. Phys. 14, 355 (1946).

2) Moss, Proc. Phys. Soc. 13, 62, 741 (1949).

3) Simpson, unpublished dissertation.

4) Hintenberger, Z. f. Physik 119, 1 (1942).

5) von Hippel and Rittner, J. Chem. Phys. 14, 370 (1946).

6) Sosnowski, Starkiewicz, and Simpson, Nature 159, 818 (1947).

7) Sosnowski, Soole, Starkiewicz, Nature 160, 471 (1947).

8) Chasmar, Nature 161, 281 (1948).

9) James, Science 110, 254 (1949).

10) Rittner, Science 111, 685 (1950).

Technical Report No. 34 - Case No. 4500
Written by:

E. S. Rittner

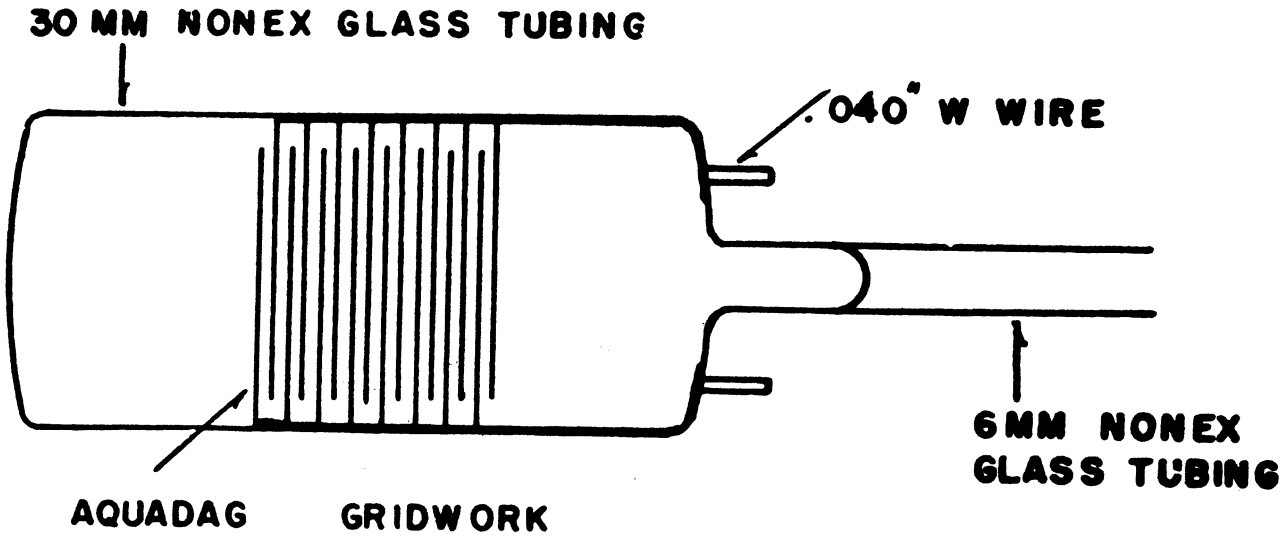
30 MM NONEX GLASS TUBING
.040" W WIRE
6MM NONEX
GLASS TUBING
AQUADAG
GRIDWORK

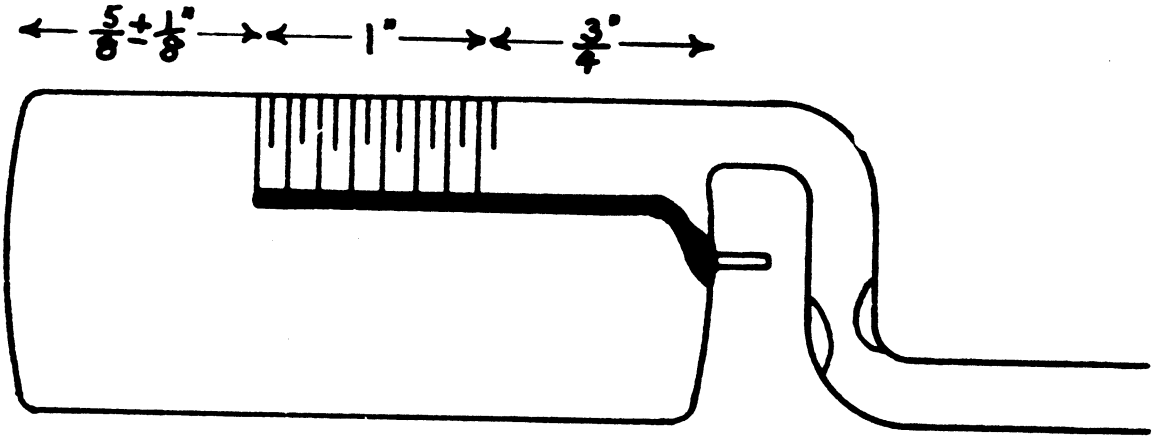
5/8 ± 1/8"
1"
3/4"

FIG. 1

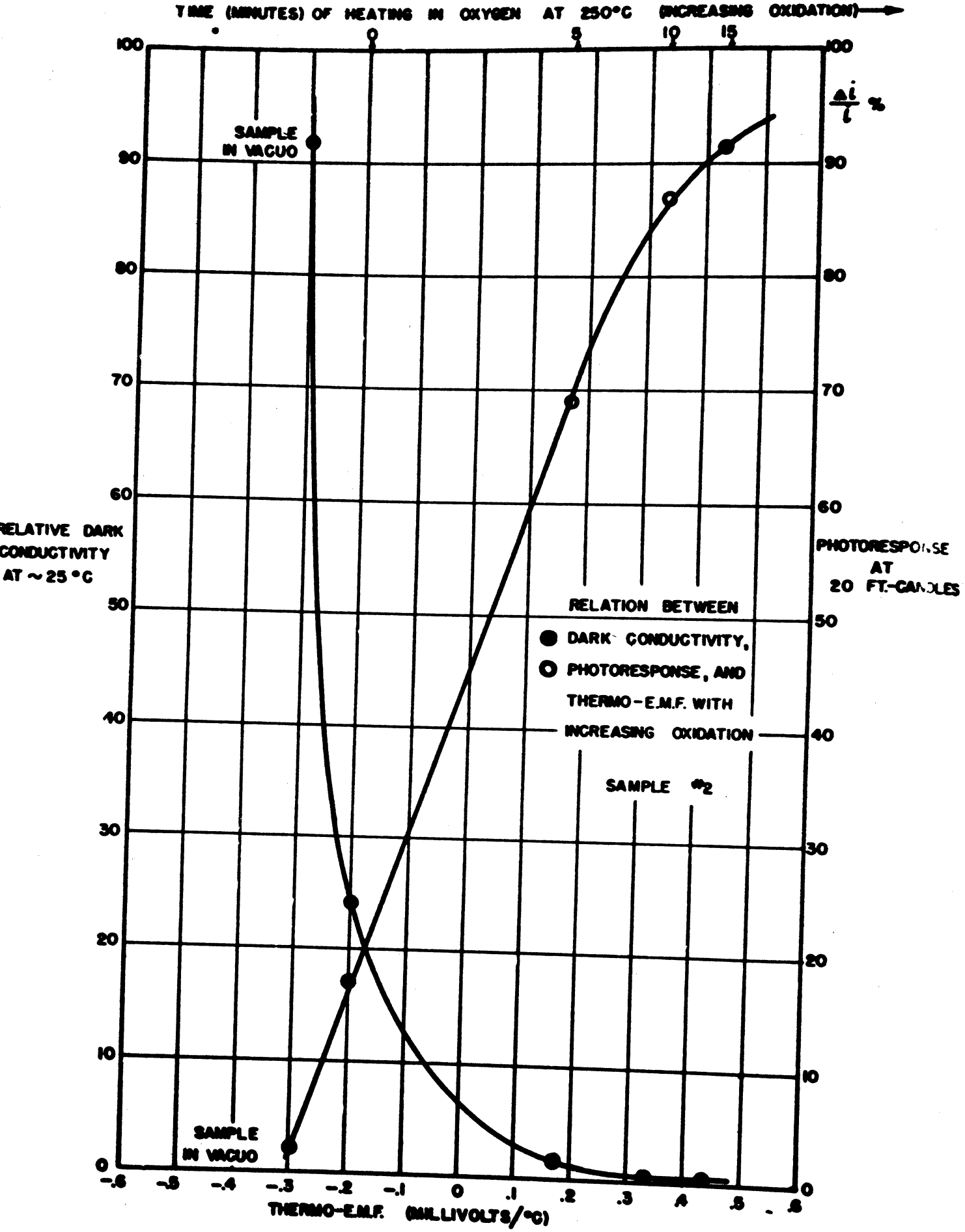
TIME (MINUTES) OF HEATING IN OXYGEN AT 250°C (INCREASING OXIDATION)
0
5
10
15
SAMPLE IN VACUO
$\frac{\Delta i}{i}$ %
RELATIVE DARK CONDUCTIVITY AT ~25 °C
PHOTORESPONSE AT 20 FT.-CANDLES
RELATION BETWEEN
DARK CONDUCTIVITY,
PHOTORESPONSE, AND
THERMO-E.M.F. WITH
INCREASING OXIDATION
SAMPLE #2
SAMPLE IN VACUO
100
90
80
70
60
50
40
30
20
10
0
-.6
-.5
-.4
-.3
-.2
-.1
0
.1
.2
.3
.4
.5
.6
THERMO-E.M.F. (MILLIVOLTS/°C)

FIG. 2

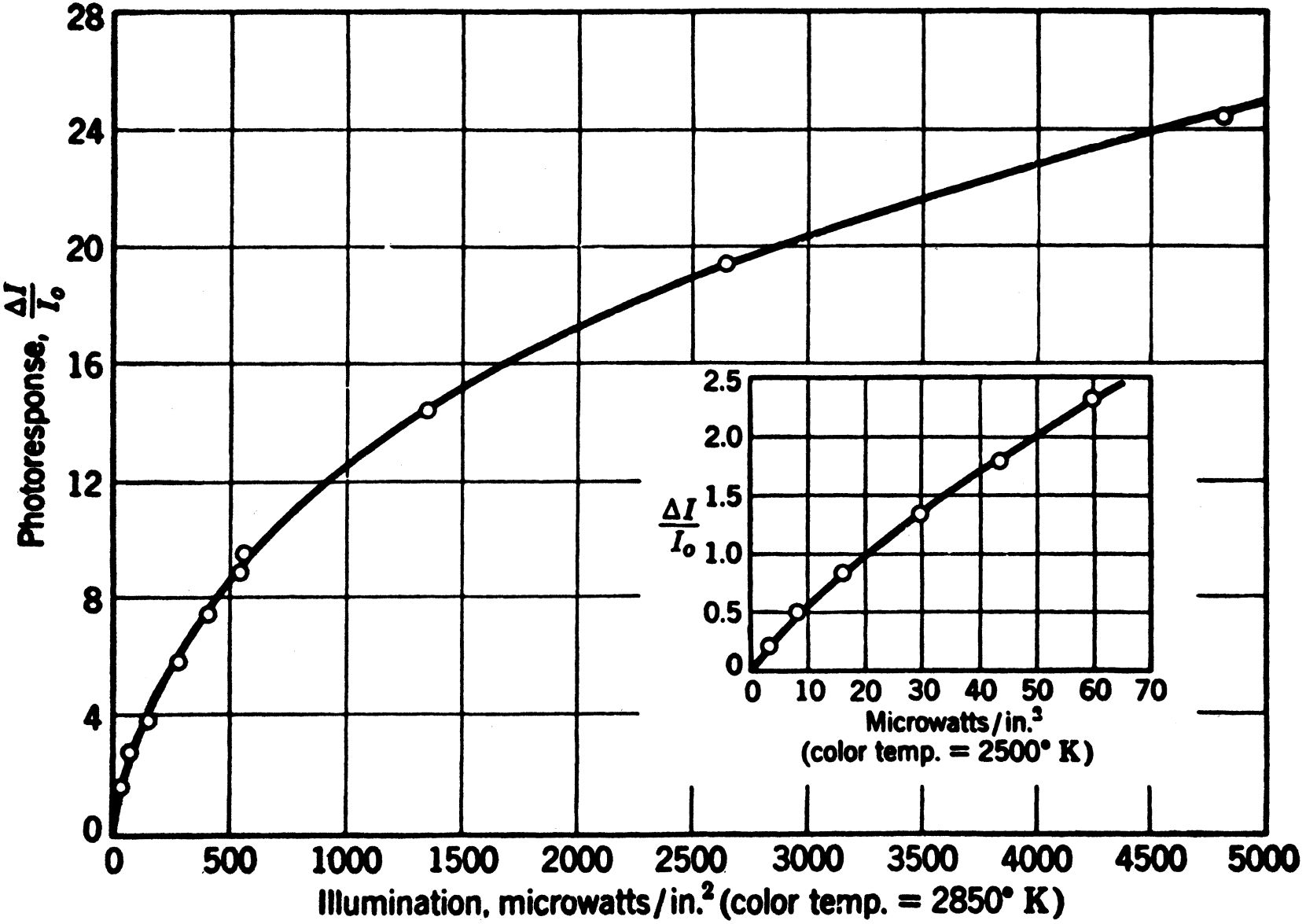

FIG. 3

Photoresponse of Thallous Sulfide Cell as Function of Intensity of Radiation. v. Hippel, Chesley, Denmark, Ulin, and Rittner

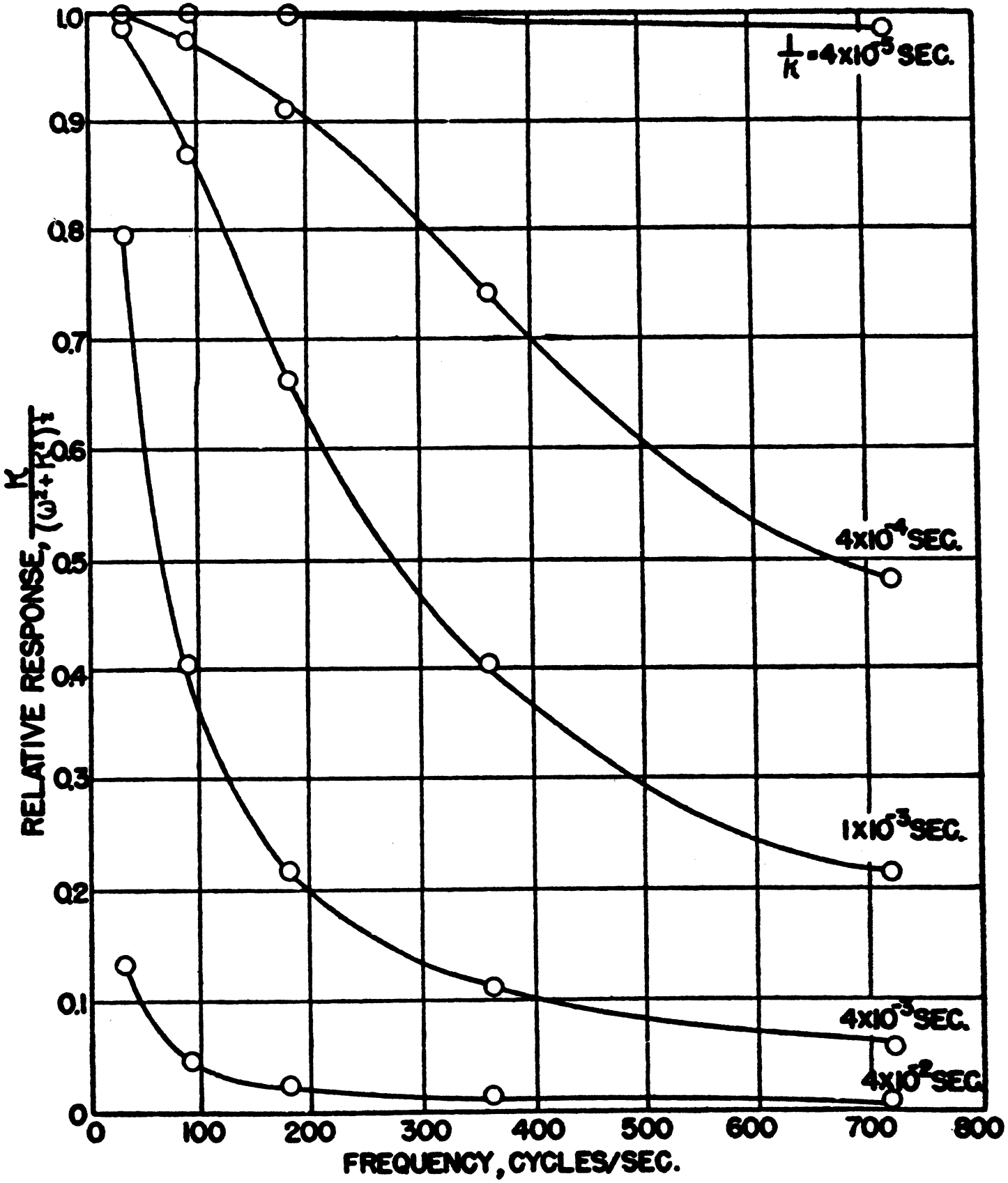

Relative response *vs.* frequency for different values of the time constant.

FIG. 4

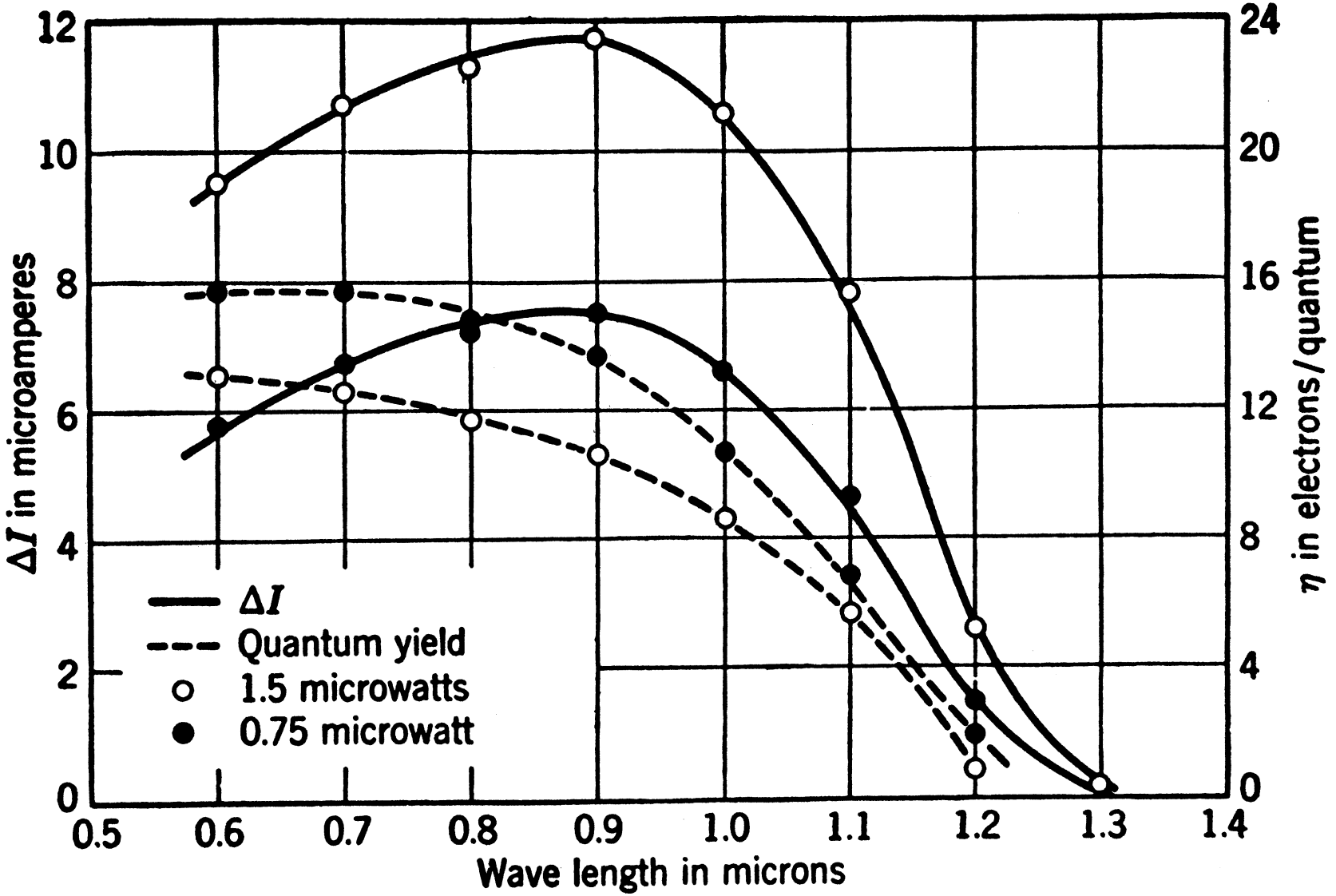

FIG. 5

Photocurrent and Quantum Yield as Function of Wave Length for Two Light Intensities (dark resistance 2.5 megohms; voltage 22.5 volts). v. Hippel, Chesley, Denmark, Ulin, and Rittner

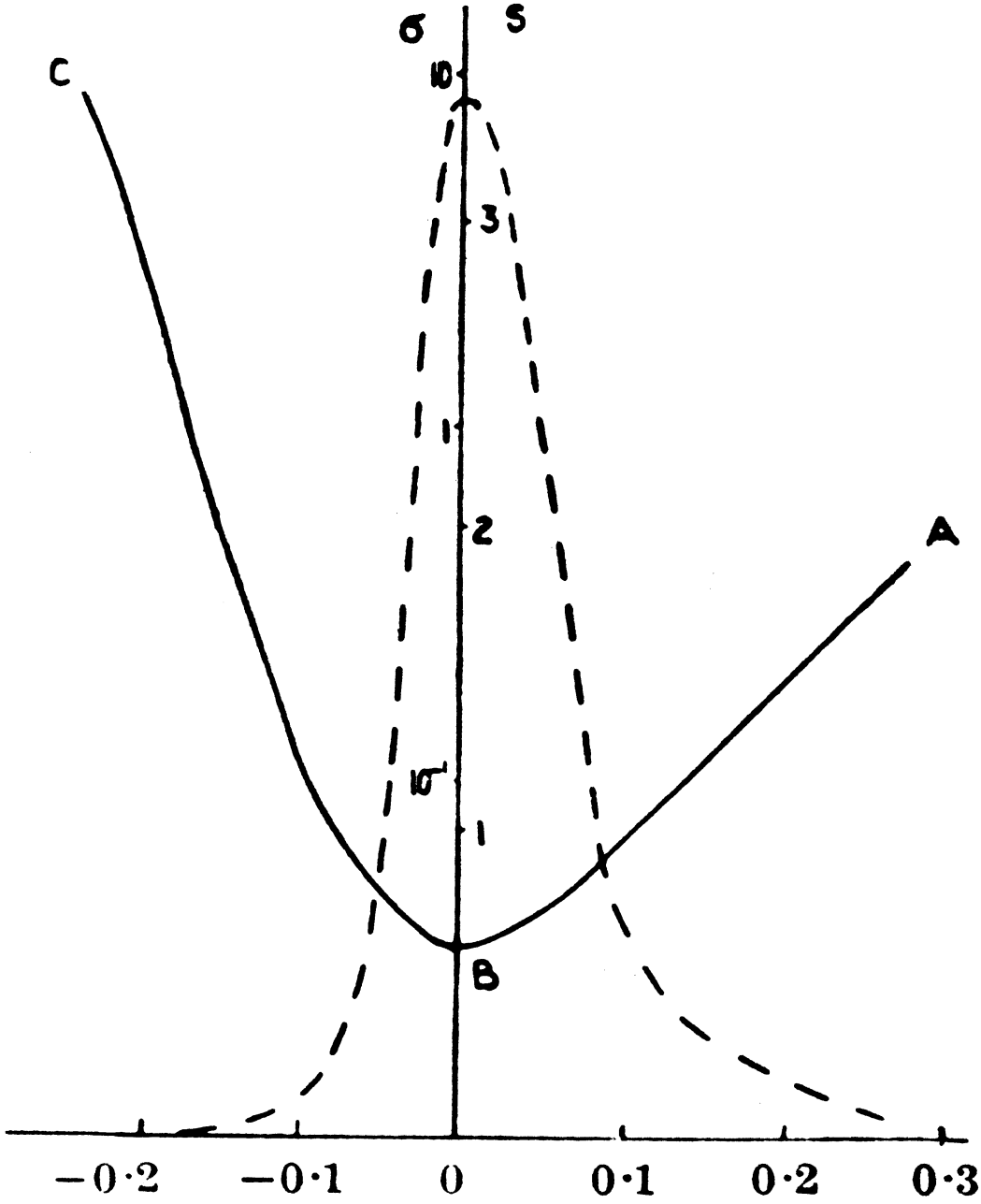

VARIATION OF CONDUCTIVITY (FULL LINE) AND SENSITIVITY (BROKEN LINE) WITH THERMO-ELECTRIC POWER

FIG. 6

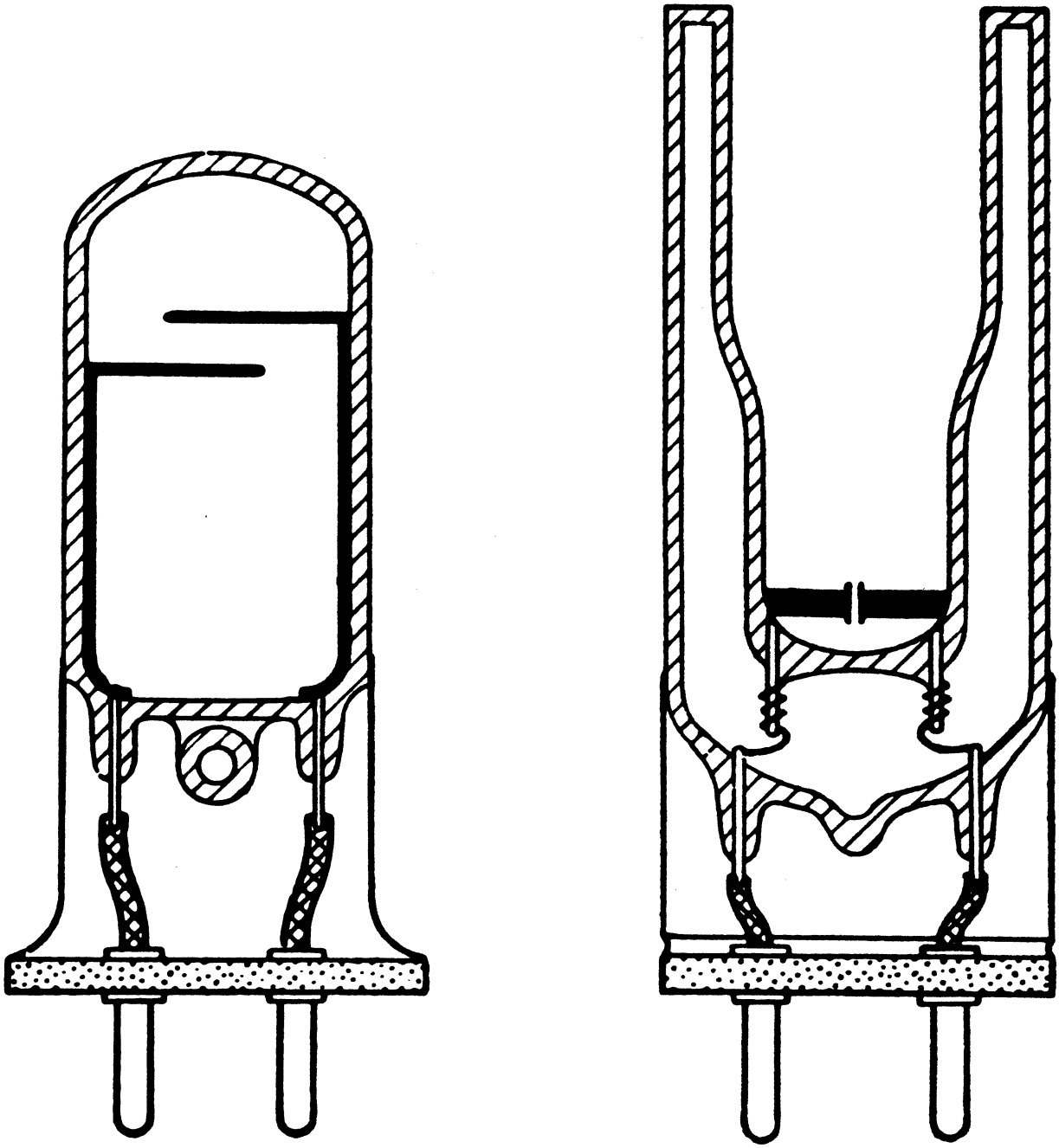

Single-Walled and Double-Walled Lead Sulfide Cells. Cashman

FIG. 7

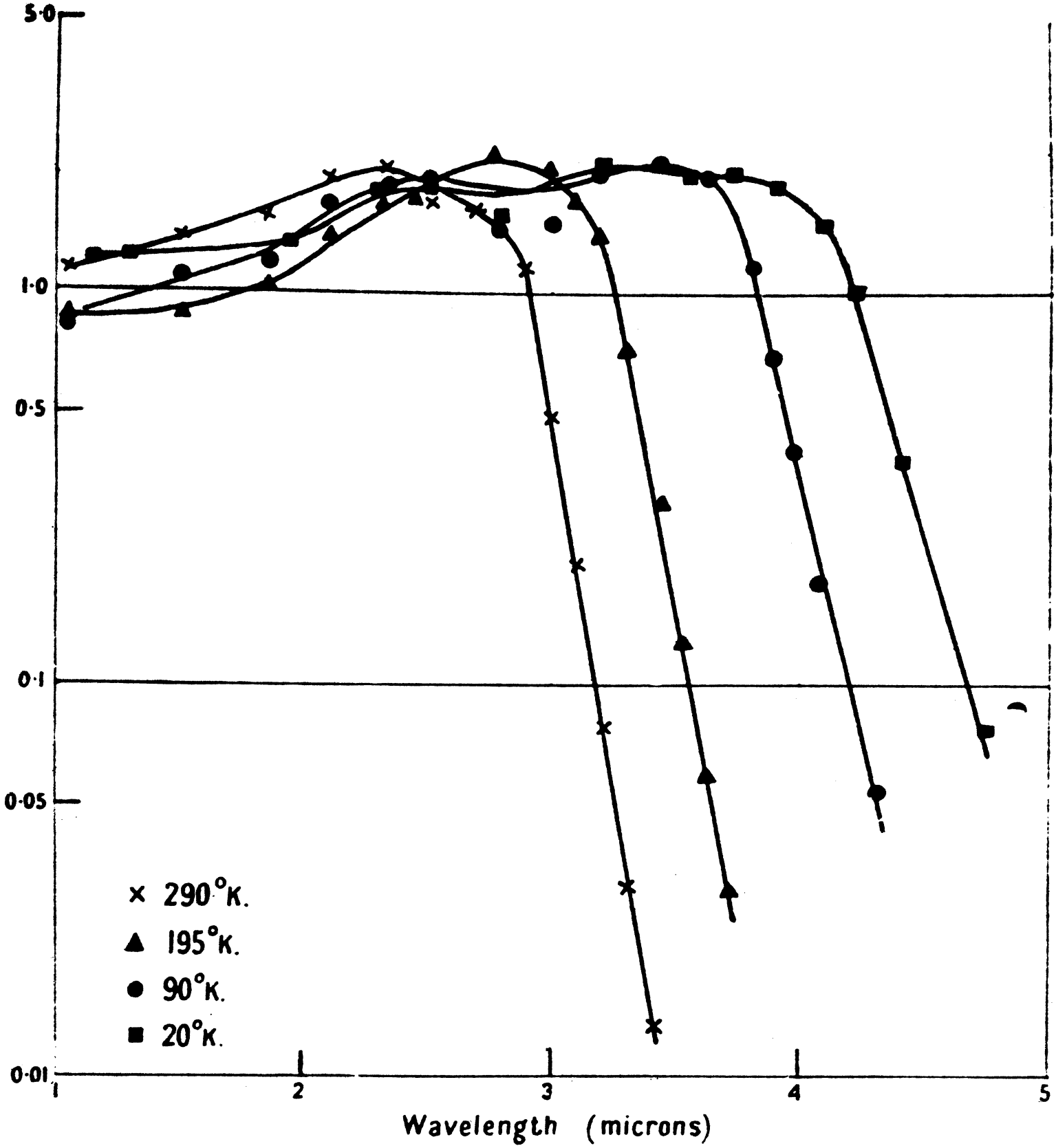
5·0
1·0
0·5
0·1
0·05
0·01
× 290°K.
▲ 195°K.
● 90°K.
■ 20°K.
1
2
3
4
5
Wavelength (microns)

FIG. 8

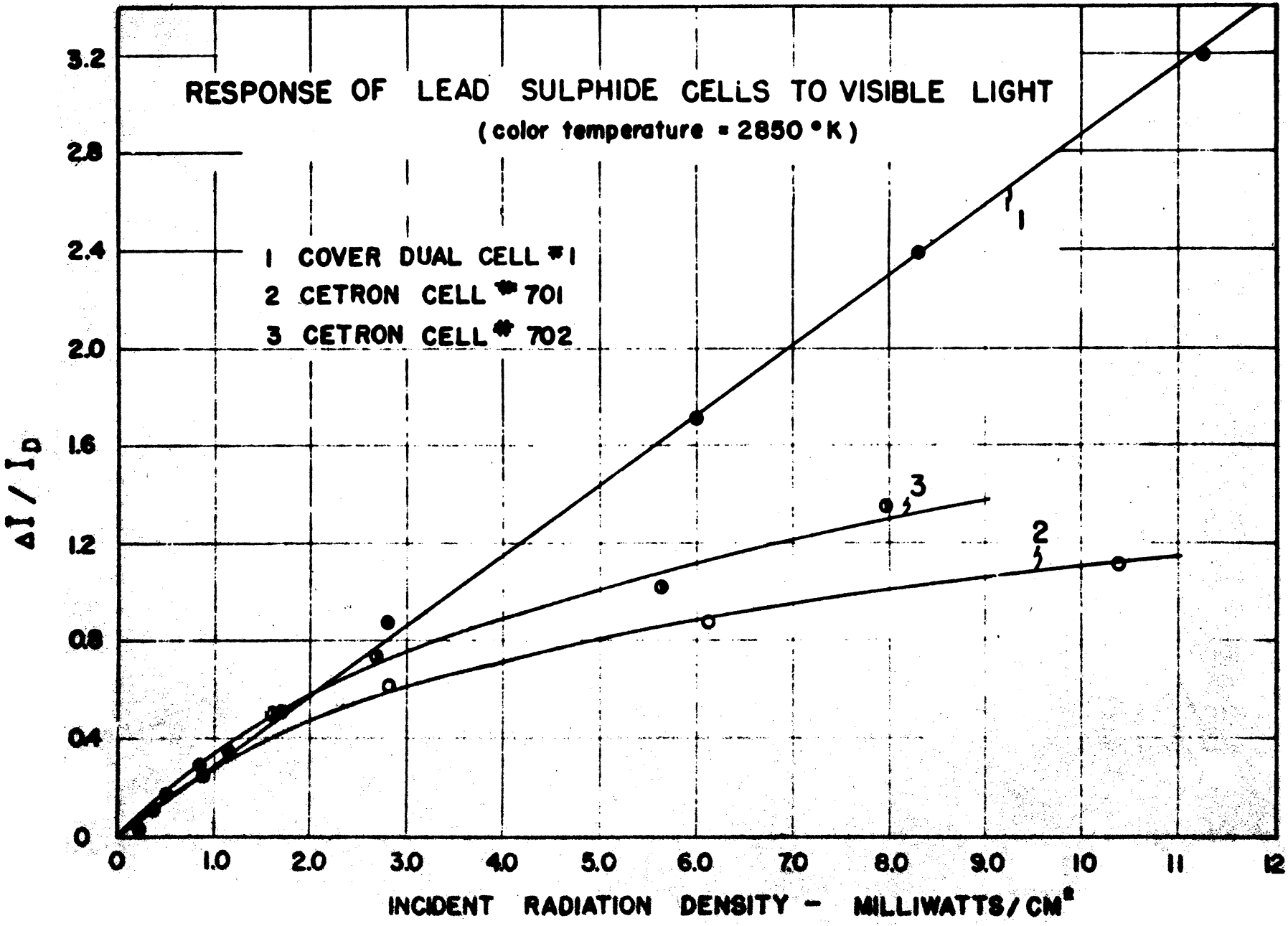
RESPONSE OF LEAD SULPHIDE CELLS TO VISIBLE LIGHT
(color temperature = 2850 °K)
1 COVER DUAL CELL # 1
2 CETRON CELL # 701
3 CETRON CELL # 702
ΔI / I_D
INCIDENT RADIATION DENSITY - MILLIWATTS / CM²
0
0.4
0.8
1.2
1.6
2.0
2.4
2.8
3.2
1.0
2.0
3.0
4.0
5.0
6.0
7.0
8.0
9.0
10
11
12

FIG. 9

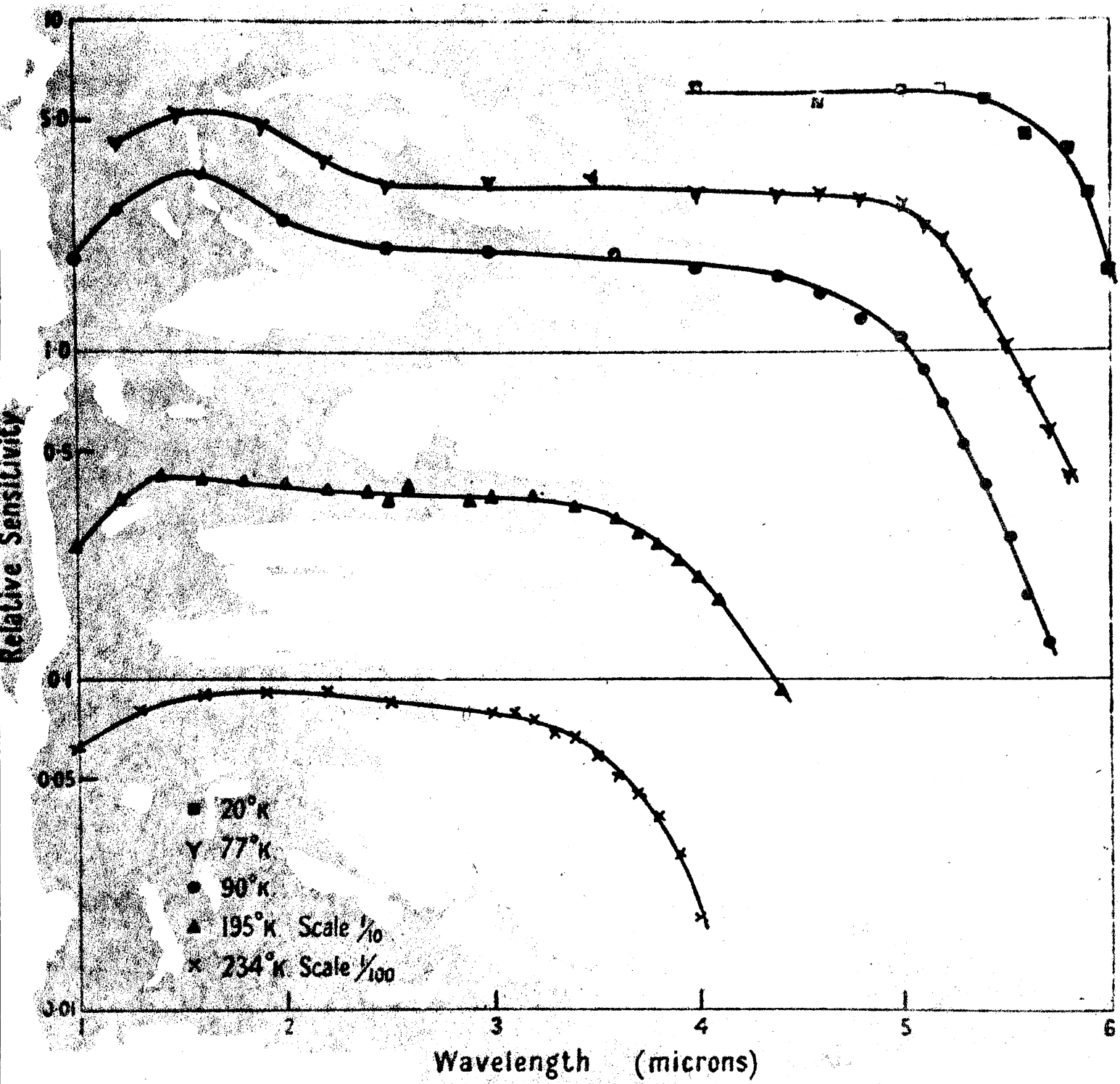

Spectral sensitivity of lead telluride.

FIG. 10

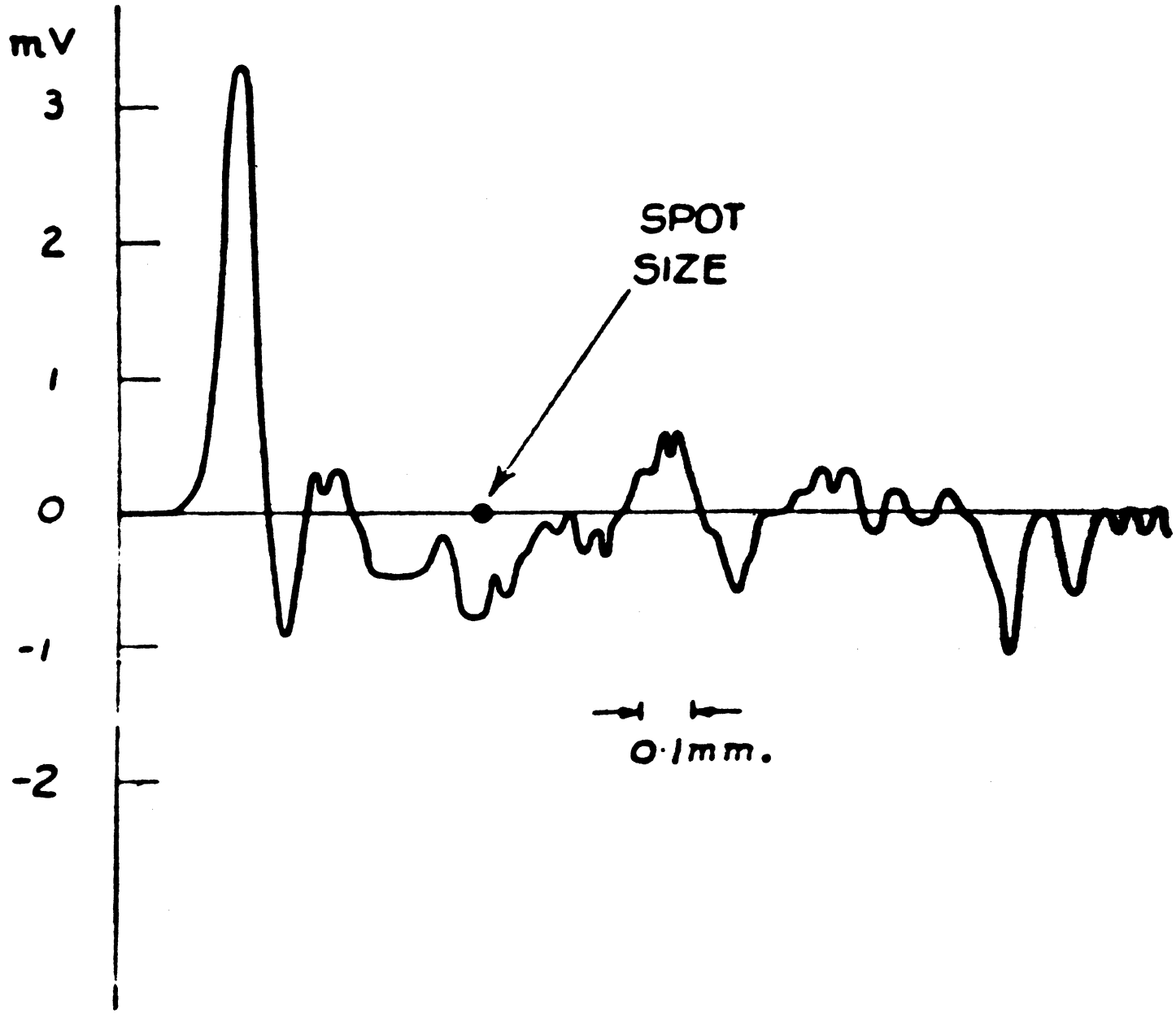

FIG. 11

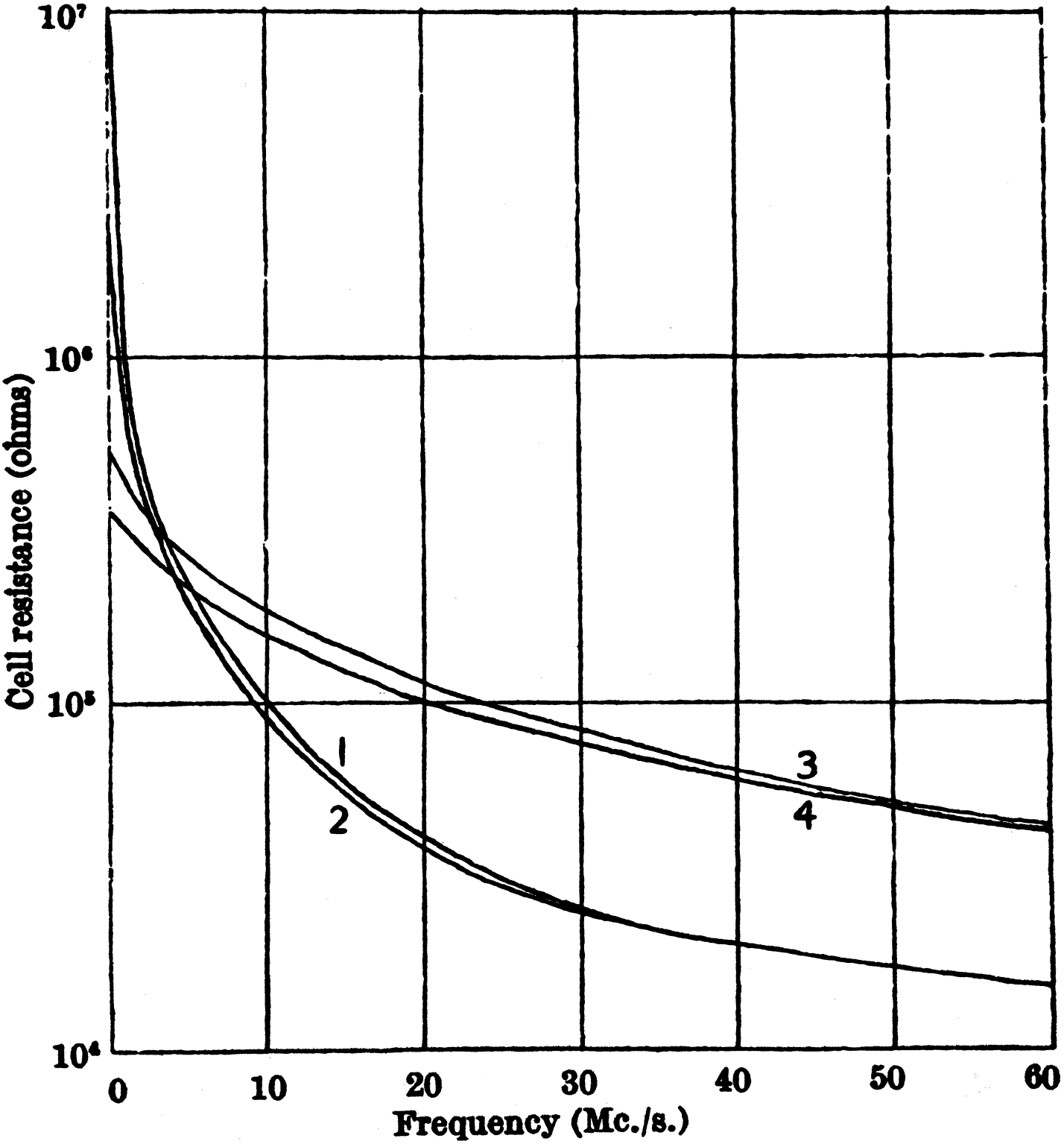

Curves 1 and 2 ; 194·5° K., cell in darkness (1), illuminated (2).
,, 3 ,, 4 ; 297° K., ,, ,, ,, (3), ,, (4).

FIG. 12

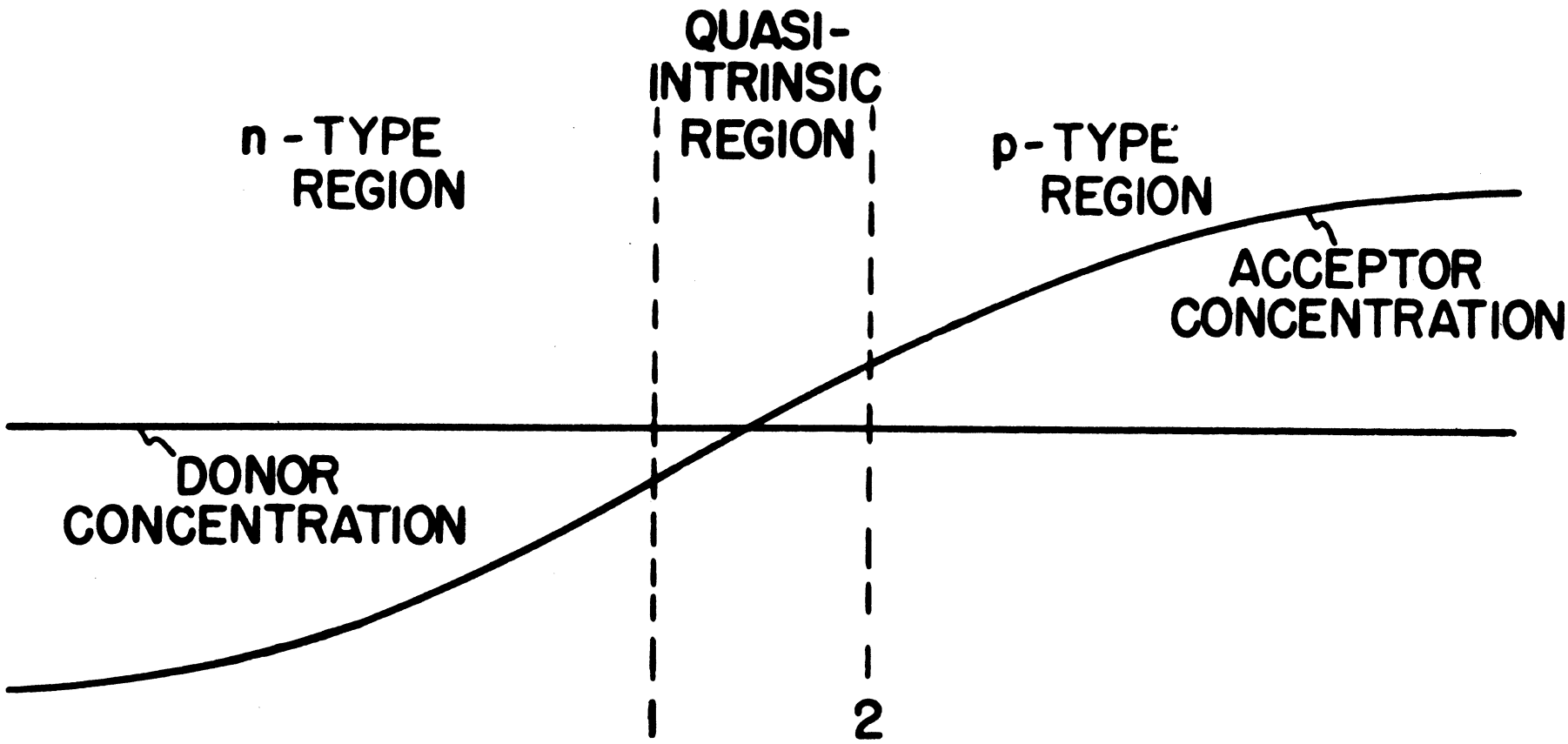
QUASI-
INTRINSIC
REGION
n - TYPE
REGION
p - TYPE
REGION
ACCEPTOR
CONCENTRATION
DONOR
CONCENTRATION
2

FIG. 13

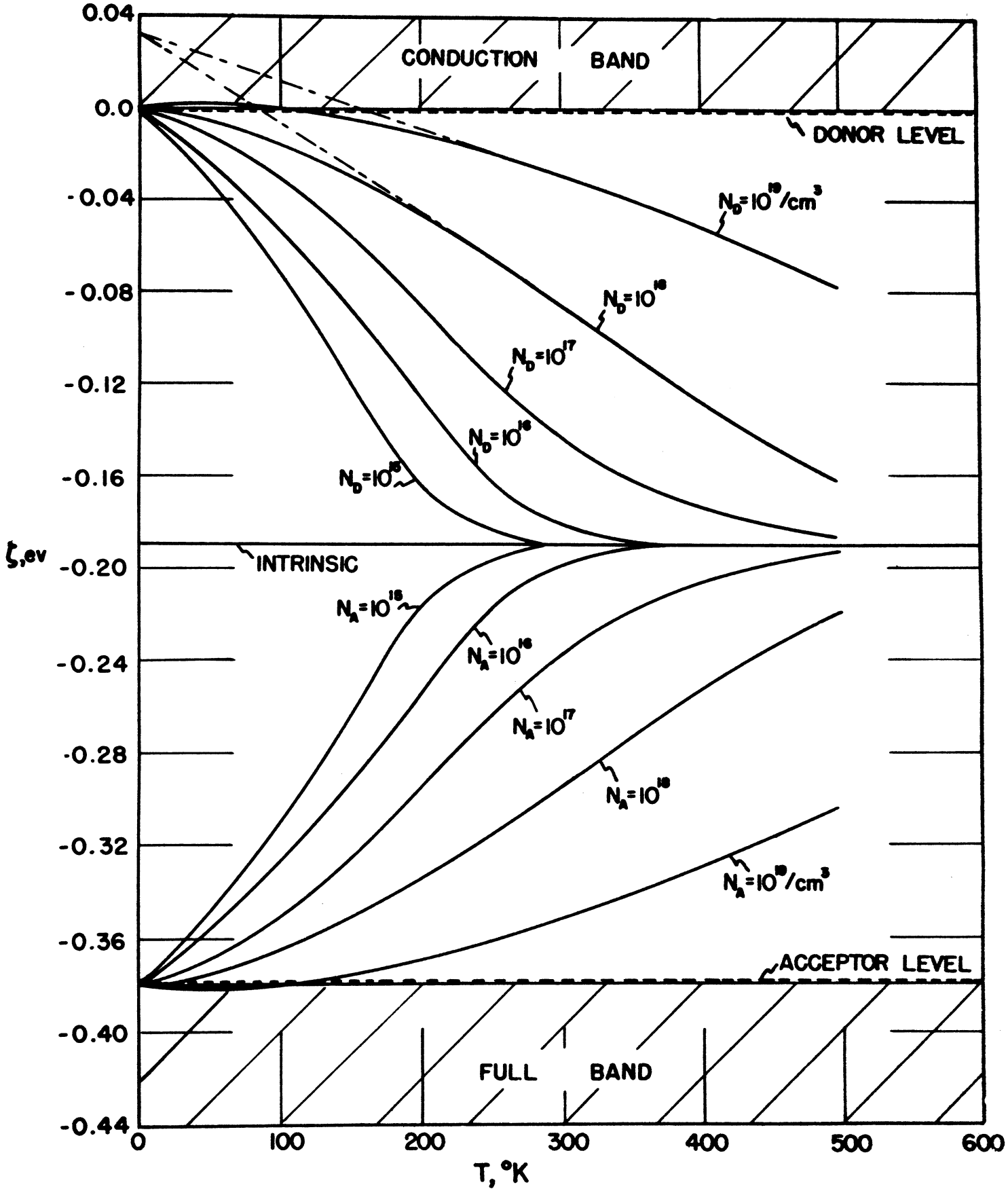

VARIATION OF FERMI LEVEL WITH TEMPERATURE AND IMPURITY CONTENT IN LEAD SULFIDE

FIG. 14

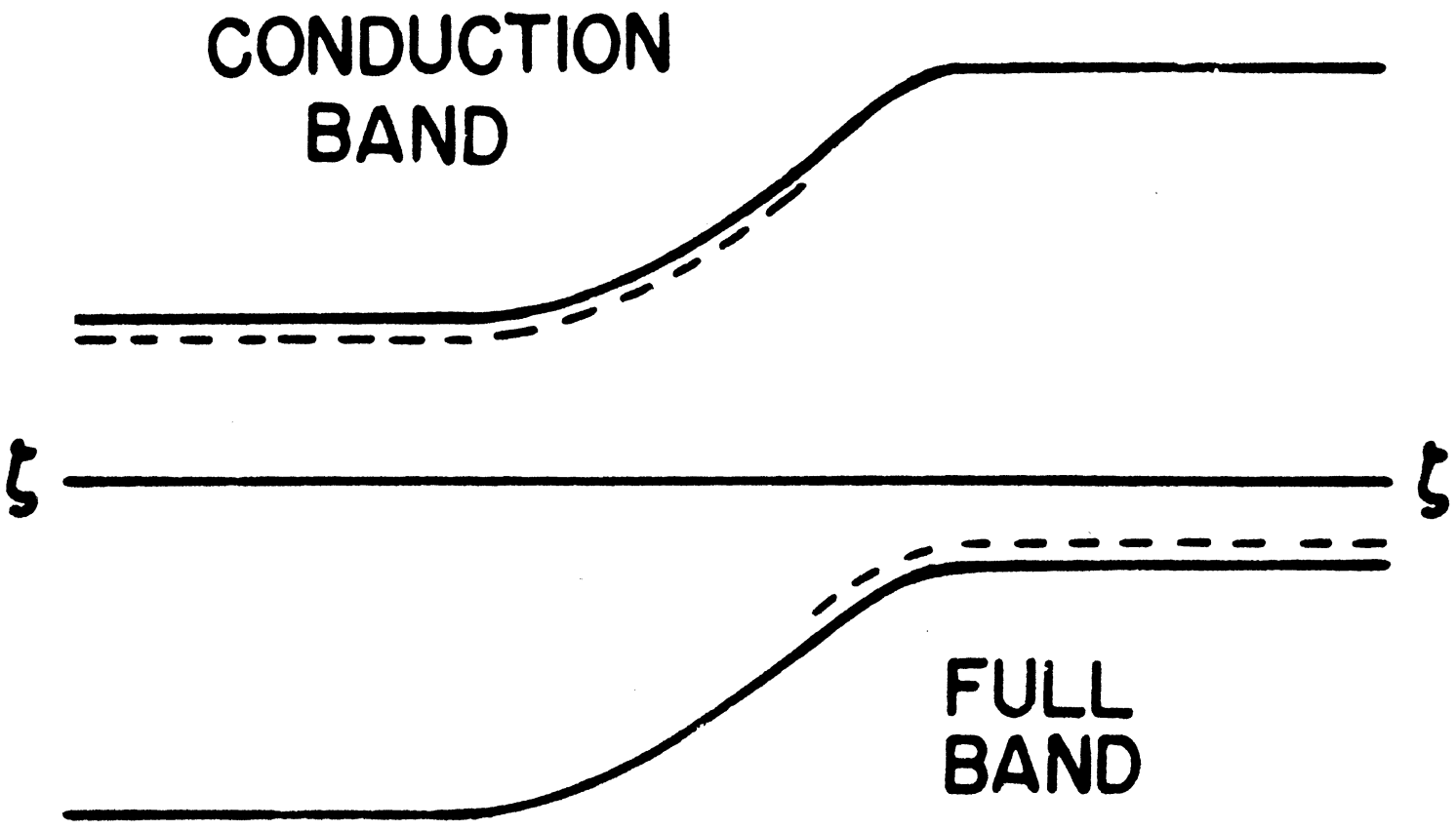

FIG. 15

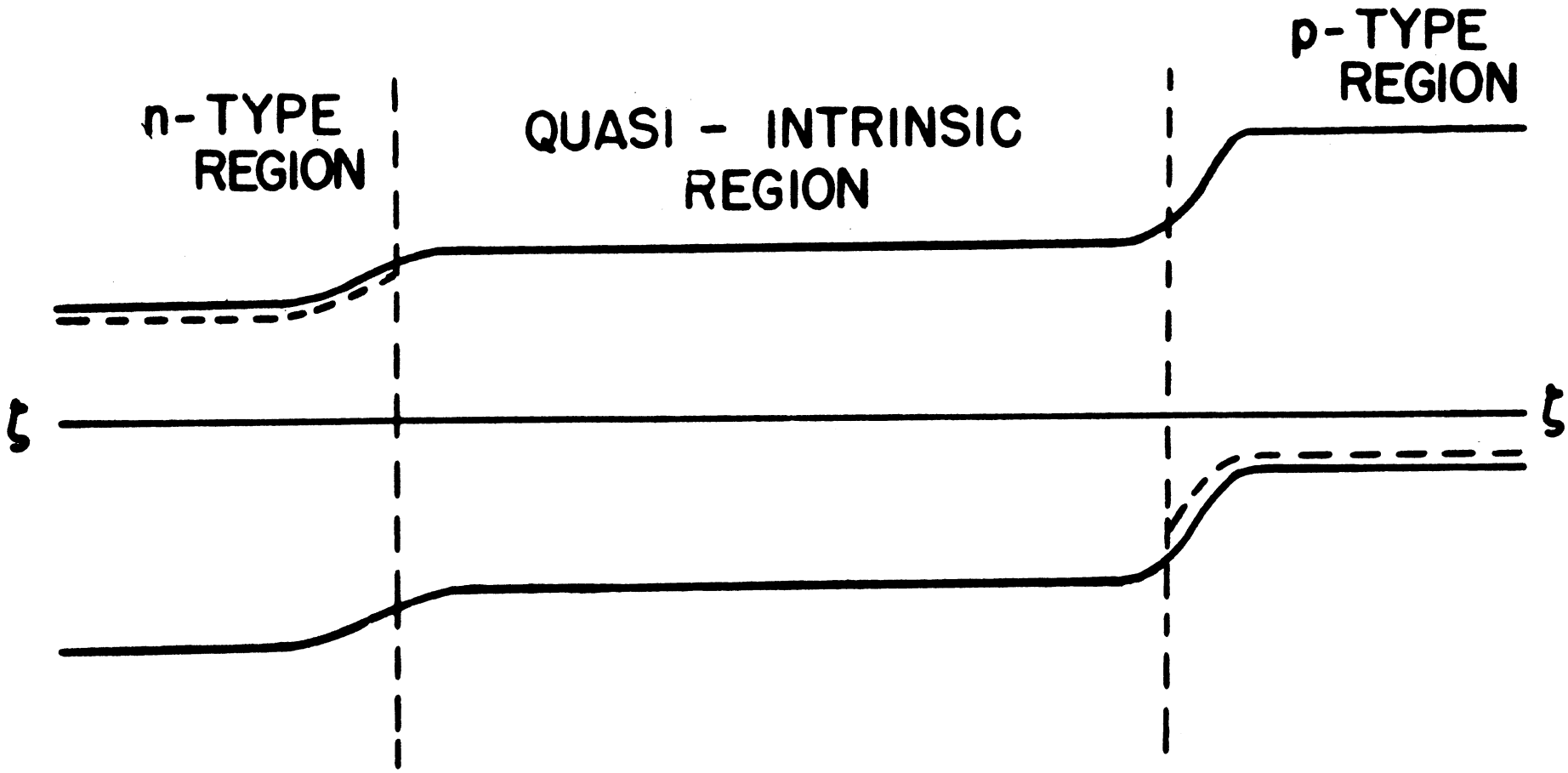

FIG. 16